CHALMERS
UNIVERSITY OF TECHNOLOGY

Electric Propulsion Active Drivetrain Oscillation Damper

Master's thesis in Systems, Control and Mechatronics

OSCAR KLANG

FABIAN LIER

DEPARTMENT OF ELECTRICAL ENGINEERING

CHALMERS UNIVERSITY OF TECHNOLOGY
Gothenburg, Sweden 2021
www.chalmers.se

Master's thesis 2021

Electric Propulsion Active Drivetrain Oscillation Damper

OSCAR KLANG

FABIAN LIER

CHALMERS
UNIVERSITY OF TECHNOLOGY

Department of Electrical Engineering
Chalmers University of Technology
Gothenburg, Sweden 2021

Electric Propulsion Active Drivetrain Oscillation Damper
OSCAR KLANG
FABIAN LIER

Supervisor: Satish Narayanan Ramachandran, Volvo Cars Corporation
Supervisor: Joachim Härsjö, Volvo Cars Corporation
Examiner: Torbjörn Thiringer, Chalmers University of Technology

Master's thesis 2021
Department of Electrical Engineering
Chalmers University of Technology
SE-412 96 Gothenburg
Sweden
Telephone +46 (0)31-772 1000

Typeset in LaTeX
Printed by Chalmers Reproservice
Gothenburg, Sweden 2021

Electric Propulsion Active Drivetrain Oscillation Damper

OSCAR KLANG
FABIAN LIER
Department of Electrical Engineering
Chalmers University of Technology

Abstract

With the introduction of electric cars, the drivetrain setup has greatly changed compared to cars with combustion engines. Due to the changed setup, external forces are more likely to trigger oscillations in the drivetrain. However, due to the fast and accurate control that the electric machine (EM) provides it should be possible to, by means of control, limit these mechanical oscillations.

In this work the possibility to damp potentially harmful mechanical oscillations in an electric vehicle drivetrain, by measuring only the EM speed, has been investigated. A plant model was built from known vehicle dynamics and several methods for observing and actively controlling the mechanical drivetrain oscillations have been reviewed and evaluated through simulations.

It has been shown that it is possible to actively damp oscillations in the drivetrain by using a recursive least squares (RLS) algorithm in combination with two different controllers and auxiliary activation logic and by measuring only the EM speed. The robustness and performance of the developed concepts have been evaluated and the results indicate that the concepts are able to damp oscillations caused by external torque transients, also for a system with varying properties. Furthermore, the results suggest that the concepts do so without otherwise negatively affecting the vehicle's performance.

For the investigated scenarios the developed proportional gain controller (P controller) achieved an average peak amplitude reduction of 63.7% in the drive shaft torsion and 76.5% in the EM speed oscillations, compared to the uncontrolled case. The developed Linear-quadratic-Gaussian (LQG) controller was able to reduce the peak amplitudes by 79.2% in the oscillations of the drive shaft torsion and 60.9% for the EM speed.

Index Terms: active torque control, drive shaft resonance, electric propulsion, mechanical drivetrain, oscillation damping, recursive least squares.

Acknowledgements

We would like to express our gratitude to our supervisors Joachim Härsjö and Satish Narayanan Ramachandran at Volvo Cars for their guidance and support throughout the project. We would also like to thank our examiner Torbjörn Thiringer for his helpful inputs and advice.

Oscar Klang and Fabian Lier
Gothenburg, June 2021

Abbreviations

ABS	Anti-lock braking system
AL	Activation logic
BPF	Band-pass filter
CAN	Controller area network
DFT	Discrete Fourier transform
EM	Electric machine
xEV	Electric vehicle
FFT	Fast Fourier transform
HPF	High-pass filter
ICE	Internal combustion engine
LQE	Linear-quadratic estimator
LQG	Linear-quadratic-Gaussian
LQR	Linear-quadratic regulator
PI	Proportional integral
PLL	Phase-locked loop
RLS	Recursive least squares
SOGI	Second-order generalized integrator

Symbols

x	Some arbitrary function or variable with unit [$\mathrm{x_{unit}}$]
$\dot{x}$	First order derivative of x [$\mathrm{x_{unit}}/s$]
$\ddot{x}$	Second order derivative of x [$\mathrm{x_{unit}}/s^2$]
$\tilde{x}$	Estimation of x [$\mathrm{x_{unit}}$]
α_{AL}	RLS bandwidth used in the activation logic [rad]
$\Delta\omega_{max}$	Upper limit for frequency change of the RLS algorithm [rad/s]
$\Delta\omega_{min}$	Lower limit for frequency change of the RLS algorithm [rad/s]
λ_{ss}	Steady state forgetting factor of the RLS algorithm [-]
λ_{tr}	Transient forgetting factor of the RLS algorithm [-]
ϕ_{EM}	Angular displacement of the EM shaft [rad]
ϕ_s	Angular displacement at the differential side of the drive shaft [rad]
ϕ_l	Angular displacement at the load side of the drive shaft [rad]
ω	Frequency [rad/s]
ω_0	Center frequency used in the BPF [rad/s]
ω_c	Center frequency used in the PLL [rad/s]
$\omega_{c,L}$	Lower cutoff frequency of the BPF [rad/s]
$\omega_{c,U}$	Upper cutoff frequency of the BPF [rad/s]
ω_{osc}	Oscillation frequency [rad/s]
ω_{osc0}	Initial assumption of the oscillation frequency [rad/s]
A_{th}	Activation threshold for the controller [rad/s]
c_s	Damping coefficient of the drivetrain [Nms/rad]
D_{th}	Deactivation threshold for the controller [rad/s]
d_{lim}	Error limit for lowering the forgetting factor of the RLS algorithm [-]
f	Frequency [Hz]
f_0	Estimation frequency of the DFT [Hz]
f_s	Sampling frequency of the DFT [Hz]
i_d	Differential ratio [-]
J_e	EM and differential lumped inertia [$\mathrm{kgm^2}$]
J_l	Total load inertia [$\mathrm{kgm^2}$]
J_w	Single wheel inertia [$\mathrm{kgm^2}$]
k_ω	Frequency estimator gain constant of the RLS algorithm [-]
k_i	PLL integral gain constant [-]
k_K	Kalman filter gain vector [-]
k_{LQR}	LQR gain vector [-]
k_p	Proportional control gain constant [Nms/rad]
k_{pll}	PLL proportional gain constant [-]
k_s	Spring constant of the drivetrain [Nm/rad]
k_{SOGI}	SOGI gain constant [-]
m_l	Load mass [kg]
N	Numbers of samples used by the DFT [-]
r_w	Wheel radius [m]
s	Complex frequency variable [$\mathrm{s^{-1}}$]
T_c	Control torque [Nm]

Symbols

T_d	Torque requested by the driver [Nm]
T_{EM}	Torque delivered to the drivetrain by the EM [Nm]
T_l	External torque acting on the wheels [Nm]
T_{net}	Net torque in the shaft at the primary side of the differential [Nm]
T_{ref}	Reference torque from the existing feedforward anti-jerk controller [Nm]
T_{req}	Total torque request to the EM [Nm]
T_s	Shaft torque at the secondary side of the differential [Nm]
$T_{s,i}$	Shaft torque at the primary side of the differential [Nm]
t	Time [s]
t_{AL}	Time constant used in the activation logic [s]
t_d	Time delay of the EM actuation [s]
t_s	Sampling time used in the RLS algorithm[s]
x_1	Torsion in the drive shaft [rad]
x_2	Angular velocity of the EM shaft [rad/s]
x_3	Angular velocity at the load side of the drive shaft [rad/s]

Contents

1
Introduction

Volvo Cars aim to reduce the environmental impact of their products and to improve the quality of air in our cities by making all-electric cars 50 per cent of their global sales by 2025, and the rest plug-in hybrids [1].

1.1 Problem background

With the introduction of electric vehicles (xEVs) the drivetrain setup has greatly changed compared to the traditional internal combustion engine (ICE) setup. The ICE drivetrain usually has a transmission with a clutch and multiple gear ratios to better utilize the limited range of efficient operating points of an ICE. Additionally it typically includes a mechanical oscillation damper installed in the drive shaft. The xEV drivetrain, on the other hand, typically has one or more electric machines (EMs) connected to the wheels through a single ratio transmission, without a mechanical oscillation damper.

Because the EM is able to provide high torque and efficiency from zero speed, varying the gear ratio might not be necessary, and instead a fixed ratio transmission can be used. Furthermore this means that a launch element, like a friction clutch, is not needed and hence it has usually been omitted in such drivetrain configurations [2]. The lack of a clutch and a mechanical oscillation damper in combination with the wide range of operation of the EM, from standstill to full speed, can result in poorly damped mechanical oscillations in the flexible shafts of the drivetrain. This will not only limit the experienced ride comfort but it can also cause significant drivetrain fatigue and wear [2].

Oscillations in the drivetrain can be triggered by external load changes due to variations in surface friction, road slope, bumps, braking, activation of the anti-lock braking system (ABS) and so on. If the frequency of such loads is close to the eigenfrequency of the drivetrain, resonance of the torque in the drivetrain can occur. If the resonance continues without being damped this can lead to oscillations with increasing amplitude resulting in discomfort, wear on the drivetrain and in extreme cases cause stability and maneuvering issues and even breakage of the drive shafts.

Traditionally, a mechanical resonance damper has been installed in the drivetrain in order to mitigate potentially harmful oscillations. Another option could be to damp them by means of active torque control of the EM. By taking advantage of the EM's

ability to react quickly and accurately, it should be possible to limit the oscillations by adjusting the torque delivered by the EM. Apart from the main goal this could also reduce cost, space, weight, design effort and potentially decreased performance, that are all side effects of adding a physical damping component. However, designing a successful torque controller is a non-trivial task that comes with challenges.

One challenge is that the only measurement available is the EM speed while the controllable input to the system is torque. Another challenge is that even though the EM reacts quickly and accurately, it does not do so instantaneously, and there will be a delay from when a torque is requested by the controller to when it is realized by the EM. A third challenge is that the measurement and control happen at the EM side of the drivetrain, while the disturbance, constituted by the external load torque, occurs at the wheel side of the drivetrain. This introduces a phase shift, and therefore the frequency and amplitude of the disturbance is unknown. A simplified illustration of the drivetrain, its components and the locations of the mentioned EM speed measurement, control torque input and disturbance can been seen in Fig. 1.1.

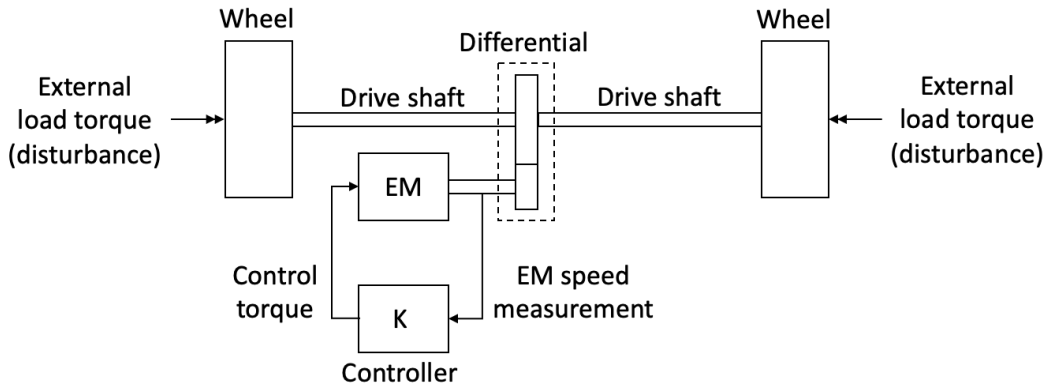

Fig. 1.1. Simplified illustration of the drivetrain including wheels, drive shafts, differential and EM. The source of the disturbance and the location of the EM speed measurement and controller is shown to support the understanding of the described system.

1.2 Previous work

A lot of previous work has been done in order to enhance comfort and driveability by reducing the longitudinal acceleration oscillations transmitted to passengers. This phenomena, called jerk, is caused by the torsional dynamics of the drivetrain during torque transients following tip-ins and tip-outs. In [3], dozens of papers regarding the state-of-the-art (2020) of automotive anti-jerk controllers are reviewed. Most, if not all, of the previous studies performed on oscillations in automotive drivetrains appear to have in common that they focus only on the effects of backlash and the longitudinal vehicle acceleration that follow abrupt changes in the powertrain torque delivery.

To the best of the authors' knowledge, there has not yet been done any studies on how to reduce the oscillations caused by the external load torque transients that a vehicle is subject to, by measuring only the EM speed, establishing the niche.

1.3 Purpose

The purpose of this project is to investigate the possibility to, by means of active control, damp potentially harmful mechanical oscillations in an xEV drivetrain, caused by external load torque transients, by measuring only the EM speed. For a concept to be considered successful in doing so, it should be able to attenuate oscillations that exceed a specified amplitude within a known range of eigenfrequencies for the drivetrain. And yet it should not unnecessarily affect the tractive torque to drive the vehicle, nor should it create an unpleasant feeling to the passenger. The ultimate aim of the controller is to reduce mechanical stress in the drivetrain, and for this reason it is the oscillations in the shaft torsion, rather than that of the EM speed, that should primarily be damped.

1.4 System, requirements and limitations

This section introduces the system under investigation and the basic assumptions, characteristics, requirements and limitations that are made throughout the project. The complete system is presented first and the individual blocks and functions are described and investigated in following chapters. Fig. 1.2 shows a schematic overview of the system as a block diagram to illustrate how the plant, controller and signals are interconnected.

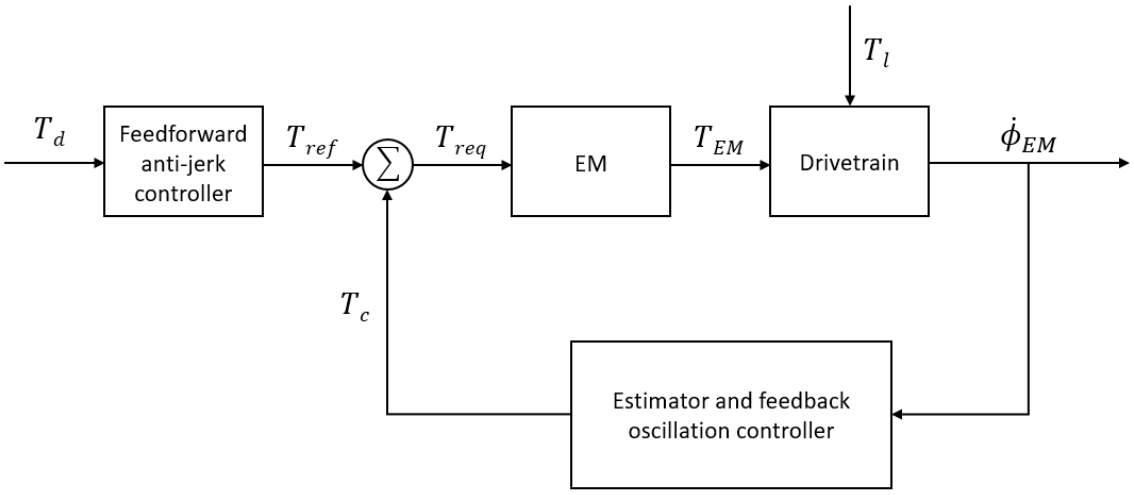

Fig. 1.2. Schematic overview of the investigated system including a signal estimation based feedback controller.

The initial input signal, T_d, is the torque requested by the driver, which is generated from the driver's input to the accelerator pedal, or alternatively by the cruise control.

The investigated vehicle, like many other xEVs, is equipped with a feedforward anti-jerk controller to mitigate shuffle phenomena, and oscillations caused by tip-ins and tip-outs are therefore not considered in this work. The effect of backlash and powertrain housing oscillations also lay outside the scope of this project.

The oscillations considered in this work are the ones caused by the external loads acting on the drivetrain. The input to the system can consequently be seen as a reference torque, T_{ref}, that will not cause oscillations in the eigenfrequency of the drivetrain. T_{ref} is assumed to be actuated and delivered to the drivetrain through the EM, although with some time delay. As this torque, T_{EM}, acts on the drivetrain, so does a disturbance caused by the external load torque, T_l, at the other end of the drivetrain. This disturbance is oscillatory in nature and results in the net torque exciting the system.

The net torque generates an angular acceleration of the EM shaft according to Newton's Second law. The corresponding angular velocity, $\dot{\phi}_{EM}$, is measured by a sensor located at the EM shaft and fed to the feedback oscillation controller. The controller to be developed in this project should incorporate a signal estimation method for extracting the oscillating component of the EM speed signal. Based on the presence of oscillations the controller should generate a damping torque, T_c, in order to mitigate oscillations in the drivetrain caused by the external load. This compensating torque should then be added to the reference torque, T_{ref}, leading to the total torque request to the EM as $T_{req} = T_{ref} + T_c$.

As mentioned, the oscillations of concern are the ones at frequencies close to the eigenfrequency of the drivetrain as they, if left uncompensated for, could amplify and potentially damage the drivetrain. Because the parameters affecting the eigenfrequency vary with time, e.g. bushings on the bearings can soften or harden with temperature, the frequency of concern is not a constant value but rather an interval. Volvo Cars have reported that their data indicate that the natural frequency is in the range of $8-12\,\text{Hz}$ for the vehicle investigated in this thesis. This is translated to requirements regarding robustness to parameter changes as follows.

The concept should be able to attenuate oscillations occurring between $8-12\,\text{Hz}$ for a drivetrain with parameters representing the same natural frequency. Simultaneously, it should be able to handle oscillations in the specified range for any given eigenfrequency without becoming unstable. It should also be robust to varying load inertia as this changes with possible passengers, cargo and trailers. Furthermore the controller should interfere minimally under normal circumstances, i.e. in the absence of oscillations within the eigenfrequency, as it might otherwise reduce the performance and associated driveability of the vehicle.

Some limitations concern the available measurements. Because adding sensors is expensive, and as the traffic on the controller area network (CAN) bus should be limited, the only measurement to be used is the angular velocity of the EM. The resolution of the sampled signal available for control action is $1\,\text{kHz}$.

Simplifications are made in order to easily model and simulate the investigated system. The drivetrain model is simplified by assuming: no wheel slip; massless shafts; lumped inertias, stiffnesses and dampings; only one EM, one wheel pair and half the vehicle inertia (this is done as there is one EM on each axis of the investigated vehicle). The time delay from when a torque is requested to when it is actuated by the EM is assumed to be constant at 3 ms. Furthermore the ratio between the torque requested and delivered is assumed to be 1:1.

1.5 Structure of the thesis

The thesis is structured into 6 chapters with corresponding sections and subsections. Chapter 1 gives a problem background, states what has previously been done and introduces the purpose and the system under investigation and some requirements and limitations that are made. Chapter 2 introduces the model used to represent the mechanical drivetrain that is used in the later chapters of the report for simulating the system and verifying the controllers. The drivetrain model is also used for model based control design. Chapter 3 gives the theory behind four different signal estimation techniques, and a comparison of the techniques is made for a set of test cases to find a method suitable for extracting the oscillatory component of a signal within a specified frequency-range. In chapter 4, different controllers are introduced and the complete system, including EM, mechanical drivetrain model, chosen signal estimation technique and different control strategies is assembled, and the controllers are compared and analysed through simulations. Chapter 5 discusses the findings and sustainability and ethical aspects and finally chapter 6 concludes the work and results and gives recommendations for future work.

2

Mechanical drivetrain model

The wheels of a car is connected to its EM through multiple components which make up the drivetrain. To allow for analysis of the relationship between the torque and speed of the wheels and EM, it is necessary to have a plant model that captures its main characteristics. Several models representing a drivetrain exist in the literature, see [4] for multiple examples, and the model complexity depends on the intended application. While higher order models could potentially achieve a higher accuracy, they are more computationally expensive to implement in controller design than a model of lower order. For this reason model based controllers often use reduced two mass models [5].

In this work a two mass system is considered to be sufficient for modelling the plant for simulations, as well as for controller implementation. In such a model, two masses or equivalent inertias, representing the EM and the load, are connected through a spring and a damper, representing the system's flexible components. In [6] it has been shown that a linear third order model achieves a close fit, in terms of capturing the main characteristics of the drivetrain, when analysing low frequency longitudinal oscillations. Such a model is visualized in Fig. 2.1.

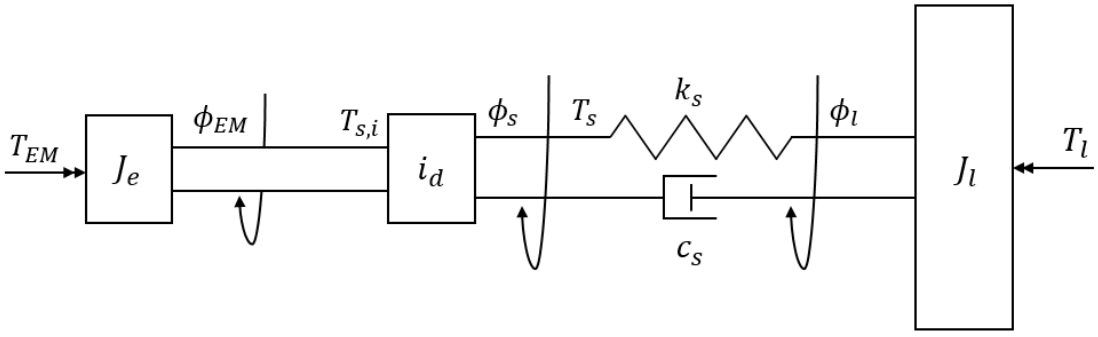

Fig. 2.1. Simple drivetrain model containing two lumped inertias, J_e and J_l, connected through a differential, with ratio i_d, by a spring and damper. The spring has stiffness k_s and the damping is c_s.

2.1 Mechanics and dynamics

In Fig. 2.1, J_e is a lumped inertia, representing the EM and the differential, subject to Newton's Second law according to

$$J_e \ddot{\phi}_{EM} = T_{EM} - T_{s,i} \tag{2.1}$$

where $\ddot{\phi}_{EM}$ is the angular acceleration of the EM, T_{EM} is the torque delivered by the EM and $T_{s,i}$ is the shaft torque at the primary (i.e. EM) side of the differential. $T_{EM} - T_{s,i}$ in (2.1) is referred to as the net torque, T_{net}. The differential has some fixed ratio, i_d, which is used for translating the angular velocity and torque. The relationship between the angular velocity of the primary and secondary side of the differential can hence be described by

$$\dot{\phi}_s = \frac{\dot{\phi}_{EM}}{i_d} \tag{2.2}$$

where $\dot{\phi}_{EM}$ is the angular velocity of the shaft at the primary side, and $\dot{\phi}_s$ is the angular velocity of the shaft at the secondary side. By assuming an ideal differential, the torque is simultaneously converted as

$$T_s = T_{s,i}\, i_d \tag{2.3}$$

where T_s is the shaft torque at the secondary side of the differential. To capture the system's damped torsional flexibility, including the damping and flexibility of all the components between the EM and the wheel's point of contact with the ground, the shaft from the differential to the wheel is modelled as a spring and damper in parallel. The spring has a spring constant, k_s, and the damper has a damping coefficient, c_s. By combining the two, the angular displacements and velocities can be associated to the torque in the drive shaft according to

$$T_s = k_s(\phi_s - \phi_l) + c_s(\dot{\phi}_s - \dot{\phi}_l) \tag{2.4}$$

where ϕ_s is the angular displacement at the differential side of the shaft, while ϕ_l and $\dot{\phi}_l$ are the angular displacement and velocity respectively, at the load side of the shaft, i.e. at the wheel. By assuming that the wheel is rolling without slip, the relationship between the angular velocity of the load (or alternatively the wheel) and the velocity of the vehicle, v_v, can be expressed as

$$v_v = r_w\, \dot{\phi}_l \tag{2.5}$$

where r_w is the wheel radius. The inertia of the wheels can then be lumped with the vehicle's mass equivalent inertia as

$$J_l = 4\, J_w + m_l\, r_w^2 \tag{2.6}$$

where J_l is the total load inertia, J_w is the wheel inertia and m_l is the mass of the load (vehicle, driver, passengers, cargo, trailer etc.). Concluding the model, Newton's Second law for the load gives

$$J_l \ddot{\phi}_l = T_s - T_l \tag{2.7}$$

where $\ddot{\phi}_l$ is the angular acceleration of the load and T_l is the load torque, constituted by the rolling resistance, air drag and road slope resistance.

2.2 State-space model

It is impractical and expensive, in terms of logistics, time and cost, to carry out tests on a real vehicle, and a plant model that allows for simulating the vehicle is usually preferable. This also enables taking a model-based development approach for controller design. With a model, it is possible to quickly simulate and test different cases and control strategies without having to implement them in a real car.

A state-space representation is a mathematical model of a physical system and is commonly used in control engineering as it provides a compact and convenient way to simulate and analyze how certain selected state variables in systems with multiple inputs and outputs change over time.

The state space model can be represented as

$$\begin{aligned} \dot{x} &= Ax + Bu \\ y &= Cx \end{aligned} \tag{2.8}$$

where x is the state vector, y is the output vector and u is the input (or control) vector to the model. A is called the state matrix, B is the input matrix and C is the output matrix.

By choosing the states to be the torsion in the drive shaft (x_1), the angular velocity of the EM (x_2) and the angular velocity of the load (x_3), the state variables are defined as

$$\begin{aligned} x_1 &= \phi_s - \phi_l \\ x_2 &= \dot{\phi}_{EM} \\ x_3 &= \dot{\phi}_l \end{aligned} \tag{2.9}$$

Manipulating (2.1) - (2.7) then yield

$$\begin{aligned} \dot{x}_1 &= \frac{x_2}{i_d} - x_3 \\ \dot{x}_2 &= -\frac{k_s}{J_e\, i_d} x_1 - \frac{c_s}{J_e\, i_d^2} x_2 + \frac{c_s}{J_e\, i_d} x_3 + \frac{T_{EM}}{J_e} \\ \dot{x}_3 &= \frac{k_s}{J_l} x_1 + \frac{c_s}{J_l\, i_d} x_2 - \frac{c_s}{J_l} x_3 - \frac{T_l}{J_l} \end{aligned} \tag{2.10}$$

where $\dot{x}_1$ is the change in torsion of the shaft with respect to time, $\dot{x}_2$ is the angular acceleration of the EM and $\dot{x}_3$ is the angular acceleration of the load.

Considering the EM torque, T_{EM}, to be a controllable input u_1, and the load torque, T_l, as an uncontrollable input u_2, and by introducing $B = [B_1\, B_2]$ and $u = [u_1\, u_2]^\top$, the state-space model representing the drivetrain can be formulated according to (2.11).

$$\begin{bmatrix} \dot{x}_1 \\ \dot{x}_2 \\ \dot{x}_3 \end{bmatrix} = \underbrace{\begin{bmatrix} 0 & \frac{1}{i_d} & -1 \\ -\frac{k_s}{J_e\, i_d} & -\frac{c_s}{J_e\, i_d^2} & \frac{c_s}{J_e\, i_d} \\ \frac{k_s}{J_l} & \frac{c_s}{J_l\, i_d} & -\frac{c_s}{J_l} \end{bmatrix}}_{A} \begin{bmatrix} x_1 \\ x_2 \\ x_3 \end{bmatrix} + \underbrace{\begin{bmatrix} 0 \\ \frac{1}{J_e} \\ 0 \end{bmatrix}}_{B_1} T_{EM} + \underbrace{\begin{bmatrix} 0 \\ 0 \\ -\frac{1}{J_l} \end{bmatrix}}_{B_2} T_l \tag{2.11}$$

2.3 Nominal plant model setup

The parameters in (2.11) are chosen to represent a generic xEV with eigenfrequency 10 Hz. The values used in the nominal plant model of the drivetrain are presented in Table 2.1.

Table 2.1: Parameters used in the nominal plant model of the drivetrain.

Parameter	Description	Value	Unit
c_s	Damping coefficient	100	[Nms/rad]
i_d	Differential ratio	8.6	[-]
J_e	Lumped EM and differential inertia	0.055	[kg m^2]
J_l	Total load inertia	160	[kg m^2]
k_s	Spring constant	15000	[Nm/rad]

As the car in this project is an all wheel drive with an EM at each axis, only half the vehicle is considered. The value of J_l presented in Table 2.1 is equivalent to a vehicle weighing 2250 kg plus a driver weighing approximately 90 kg ($m_l \approx 2340$ kg), and with a wheel radius $r_w = 365$ mm and wheel inertia $J_w = 2$ kg m^2 according to (2.6).

2.4 Analysis

The modelled system is analyzed in the time and frequency domain in order to investigate how input torque from the EM and from the wheel side of the drivetrain influence the drive shaft torsion and EM speed. MATLAB and Simulink are used for simulating.

First the transfer functions of the state space model in (2.11) are analyzed by studying their bode diagrams, see Fig. 2.2 - 2.3. Then measurements from a test vehicle are reviewed in Fig. 2.4 - 2.5, and finally the open loop behaviour of the plant model is analysed through simulations, see Fig.2.6.

As can be seen in Fig. 2.2 the bode diagrams from EM and load torque to shaft torsion reveal that the torsion in the drive shaft has a magnitude peak at around 10 Hz for a torque applied at either ends of the drivetrain. The system is designed to have an eigenfrequency at 10 Hz, hence this is expected. The phase is the same regardless of the torque origin.

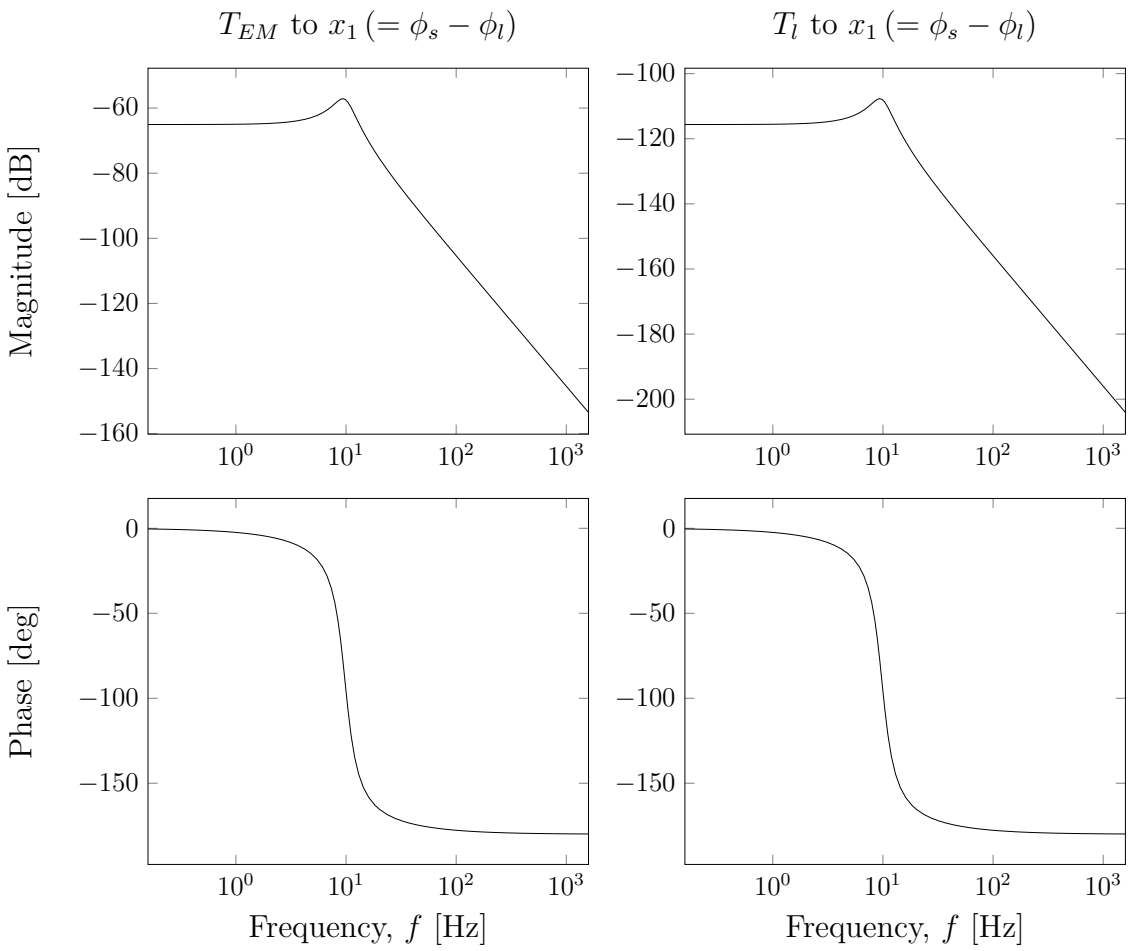

Fig. 2.2. Bode diagram from EM and load torque to shaft torsion showing the resonance peak at 10 Hz.

From Fig. 2.2 it is also observed that the magnitude of the torsion is higher from torque applied at the EM than for torque applied at the load. The reason for this is that the torque applied at the wheels is subject to a much larger inertia than the EM torque (see Table 2.1). Also the EM torque is amplified through the differential resulting in greater impact on the torsion.

The parameters that have a significant impact in determining where the resonance frequency, f_r, is located are: the spring constant k_s, the equivalent EM and differential inertia J_e and the differential ratio i_d. The resonance frequency can be approximated according to

$$f_r \approx \frac{1}{2\pi}\sqrt{\frac{k_s}{J_e\, i_d^2}} \tag{2.12}$$

For the investigated system i_d is a known constant and J_e is considered to be a constant with some neglectable deviation, mainly owing to manufacturing tolerances. Variations in the eigenfrequency of the drivetrain is thus assumed to mainly stem from alteration in the shaft stiffness k_s. The model assumes an equivalent or

lumped value for the stiffness, representing all the flexible components in the drivetrain. However this assumption is a simplification as the real system's stiffness can vary with temperature in the flexible components, tire-pressure, friction and other nonlinearities that the model does not detain.

As the only measurement available for control feedback is the EM speed it is of interest to see how it is affected by the inputs to the system. Fig. 2.3 shows the bode diagram from T_{EM} and T_l to EM speed, $\dot{\phi}_{EM}$.

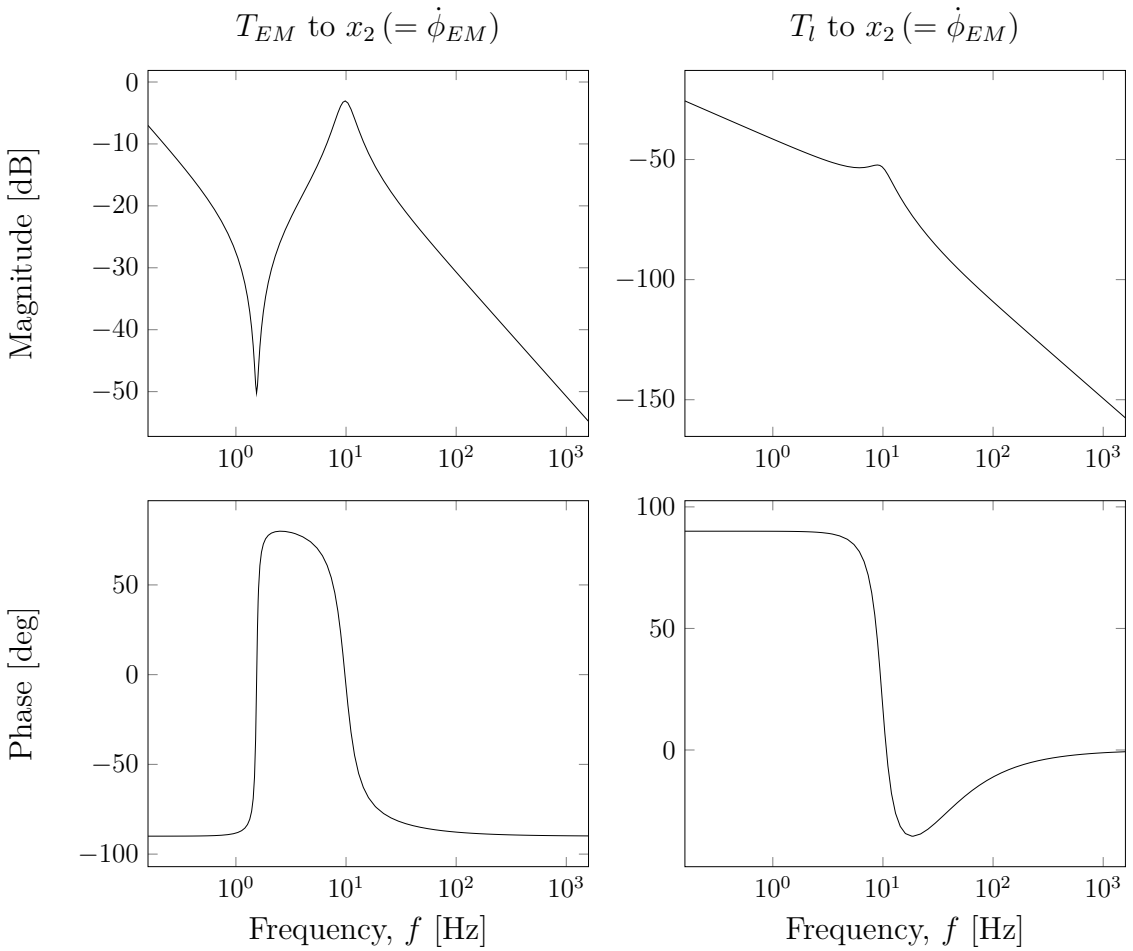

Fig. 2.3. Bode diagram from EM and load torque to EM speed showing the resonance peak at 10 Hz.

As can be seen in Fig. 2.3 the magnitude peaks around 10 Hz are present also in the angular velocity of the EM, indicating that the resonance phenomena can be observed through measurements from the EM speed. Torques originating from either side of the drivetrain with frequencies coinciding with the natural frequency of the drivetrain are amplified to the EM speed. However, the resonance peak from the load torque is not as distinguishable in the EM speed as it is in the shaft torsion. This gives an indication that a controller with access to a wheel speed measurement as well as that of the EM could perform better, as the torsion could then be determined in each time step.

The frequencies at the EM speed that correspond to resonance in the drivetrain are verified by studying real measurements of the EM speed in a test vehicle equipped with torque sensors at the drive shafts. The resonance has been confirmed by the oscillating torque in the shafts and the correlated EM speed is presented in Fig. 2.4.

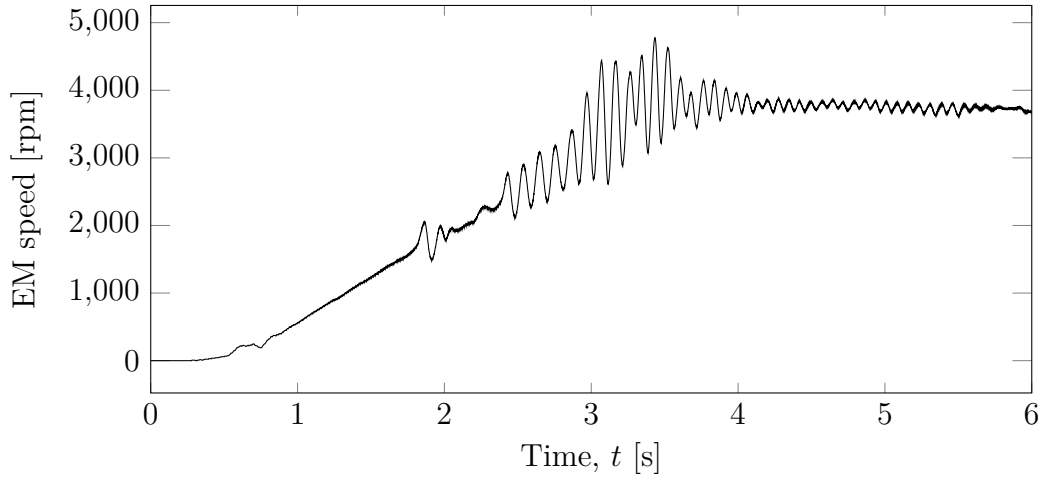

Fig. 2.4. EM speed measurement from a test vehicle equipped with torque sensors on the drive shafts. Resonance in the drive shaft torque has been confirmed in the test.

In the measured signal seen in Fig. 2.4 the EM speed is rapidly increased from $t \approx 0.5\,\text{s}$ and at $t \approx 2.5\,\text{s}$ the angular velocity of EM starts to fluctuate and ends in oscillations with amplitudes up to 1000 rpm. In order to investigate the frequencies of the oscillations the equivalent power spectrum seen in Fig. 2.5 is studied.

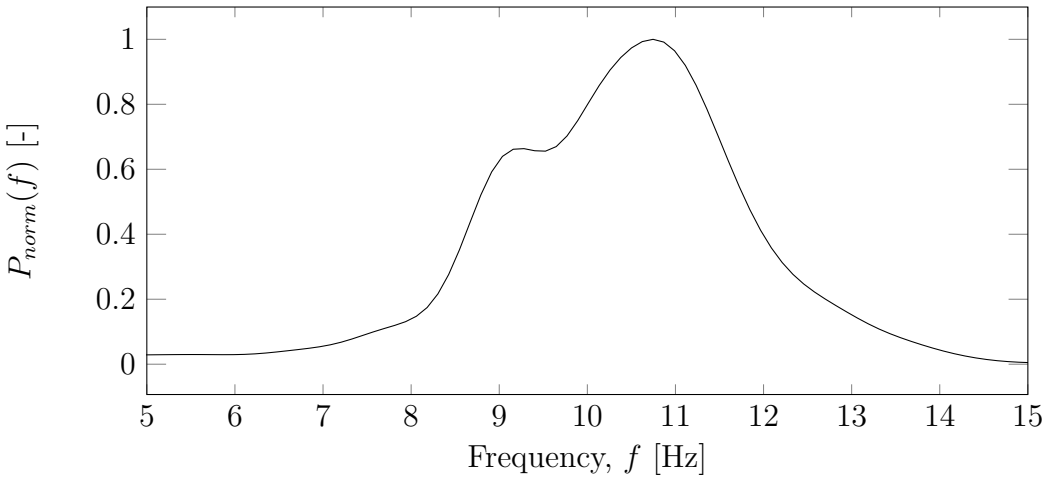

Fig. 2.5. Power spectrum of the measured EM speed in Fig. 2.4 for frequencies between 5 and 15 Hz. The power is normalized according to $P_{norm}(f) = \frac{P(f)}{P_{max}(f)}$, where f is the frequency and $P_{max}(f)$ is the maximum value of $P(f)$.

The power spectrum seen in Fig. 2.5 reflects the amplitude of the EM speed oscillations present at different frequencies. It is evident that the critical frequencies for the test vehicle does in fact lay in the range of $8-12\,\text{Hz}$.

In order to visualize and verify that the drivetrain model in (2.11) can be representative for the real system in terms of amplified shaft torsion in the eigenfrequency it is implemented and studied using Simulink. Many cases and scenarios are tested and analyzed. In Fig. 2.6 the open loop response of the plant model for a specific case, that is considered to seize the main characteristics, is presented.

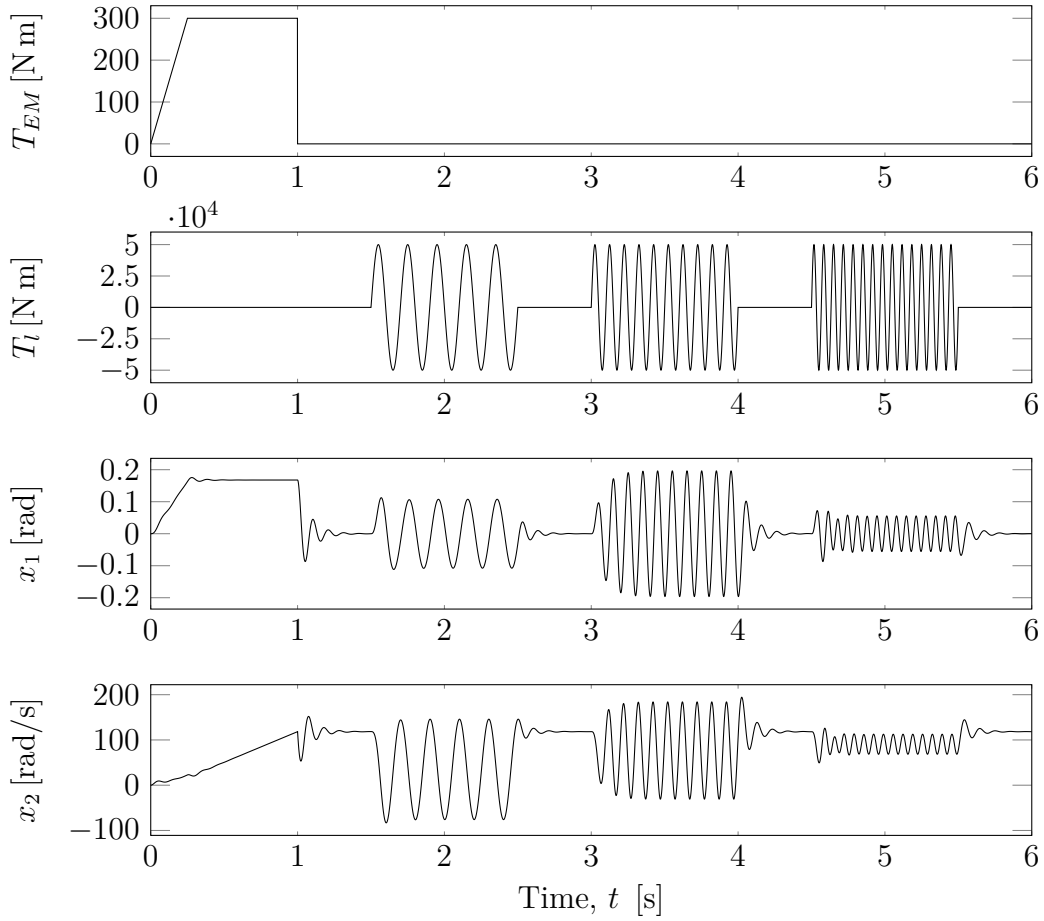

Fig. 2.6. Simulation of the drivetrain visualizing how sinusoidal load torques of three different frequencies (5, 10 and 15 Hz) are passed through the model to the drive shaft torsion (x_1) and EM speed (x_2).

As seen in Fig. 2.6 the EM torque is ramped up and kept at a constant 300 N m for the first second, while the load torque is kept at 0 N m. The torsion in the drive shaft (x_1) roughly follows the shape of T_{EM} while the EM speed (x_2) increases until T_{EM} is abruptly decreased to 0 at $t = 1$ s. When studying the shaft torsion and EM speed for the first 1.5 seconds, the shuffle phenomena widely covered in the literature, see e.g. [7], can be observed when the torque applied by the EM is changed rapidly, causing oscillations in both states. As mentioned in chapter 1.4, this is taken care of by the existing feedforward anti-jerk controller in a real case, and is not considered in this work. Note that there is no such controller included in the plant model that is used for the simulations in this work, and hence the shuffle can be seen in Fig. 2.6. However, they would not be there in a test carried out in a real car.

After $t = 1\,\text{s}$ the EM torque is kept at 0 while a sinusoidal load torque of varying frequencies is applied in intervals of 1 s in order to examine the transfer to the shaft torsion and EM speed. The amplitude of T_l is constant at $50\,000\,\text{N m}$ for the three intervals while the frequency $f(t)$ is varied as $f(t{=}1.5{:}2.5) = 5\,\text{Hz}$, $f(t{=}3{:}4) = 10\,\text{Hz}$ and $f(t{=}4.5{:}5.5) = 15\,\text{Hz}$. When studying the torsion in the drive shaft it can be seen that the 5 Hz signal generates oscillations with a constant amplitude of 0.1 rad while the torque of 10 Hz has its first peak at 0.1 rad before it amplifies resulting in amplitudes of 0.2 rad. This indicates that the eigenfrequency is excited, i.e. resonance has been triggered, leading to intensified torsion in the shaft of magnitudes twice as high as for the 5 Hz case. For the 15 Hz signal, the amplitude is damped compared to the 5 Hz signal, generating amplitudes of 0.05 rad.

The EM speed appears to be oscillating at similar amplitudes for the 5 and 10 Hz signals but a buildup in the amplitude can somewhat be noticed in the 10 Hz case. The 15 Hz oscillations are damped in relation, as was observed in the shaft torsion. These results are all as expected and agrees with what is shown in the bode diagrams in Fig. 2.2 - 2.3.

2.5 Summary

Known vehicle dynamics were used to represent a drivetrain as a two mass spring damper system. The plant model was put into a state-space representation in order to simulate and investigate the model. By analyzing the transfer functions from the torque inputs to the shaft torsion and EM speed, and by visualizing the signals, it has been verified that the model acts as expected and captures the resonance in the drive shaft for load torques applied at frequencies coinciding with the eigenfrequency of the drivetrain. The oscillations at critical frequencies, regarding resonance in the torsion of the shaft, can be observed through the EM speed. However, the oscillations within the eigenfrequency are not as clearly amplified in the EM speed as they are in the torsion, if comparing the 5 and 10 Hz cases. This motivates the use of some filtering technique for further highlighting the critical frequencies in the EM speed measurement.

3

Signal estimation techniques

In chapter 2 it was stated that the critical frequencies in the EM speed measurement signal should be highlighted in order to separate them from non-critical frequencies. In this chapter four different methods for distinguishing the oscillatory component within a certain frequency range of a signal are investigated and compared in order to find a technique suited for an active drivetrain oscillation damping controller.

The only measurement to be used for feedback control is the angular velocity of the EM. In order to detect resonance in the drive shaft, the frequency components close to the eigenfrequency of the drivetrain should be extracted from the measurement signal. By doing so, a signal potentially suitable for control action is retrieved. By monitoring the frequency and amplitude of the extracted signal, a window function can be used for activating and deactivating a controller. The controller should be turned on if the frequency and amplitude of the signal lay within the frame of the defined window, and otherwise turned off.

In order to prevent damage to the drivetrain it is important that the controller is activated quickly if resonance in the drive shaft is detected. At the same time, the controller should interfere minimally in the absence of resonance, as it might otherwise reduce performance and driveability. This means that the signal estimation technique needs to be fast and accurate in tracking and distinguishing the critical frequencies. Therefore, the signal estimation techniques described in this chapter are tuned to amplify frequencies in the range of $8-12\,\text{Hz}$ while attenuating all other frequencies.

A set of signals are used for calibrating and fine-tuning each filtering method by considering settling time, frequency selectivity, phase and amplitude accuracy, and overall performance and stability. The parameter values that are ultimately chosen for each method are presented in the respective setup sections.

3.1 Band-pass filter

A common filtering technique used in a wide variety of applications is the band-pass filter (BPF). As the name implies it is used to only pass, or extract, frequencies within a certain frequency band, while attenuating frequencies outside the band range. In [8] a second order BPF in Laplace notation is described as

$$\frac{\frac{\omega_0}{Q}s}{s^2 + \frac{\omega_0}{Q}s + \omega_0^2} \tag{3.1}$$

where

$$Q = \frac{\sqrt{\omega_{c,U}\,\omega_{c,L}}}{\omega_{c,U} - \omega_{c,L}} \tag{3.2}$$

and ω_0 is the frequency proportionate to a filter gain of 1. The Laplace symbol s $(= j\omega)$ is the complex frequency variable. $\omega_{c,U}$ is the upper cutoff frequency while $\omega_{c,L}$ is the lower equivalent, as can be seen in Fig. 3.1.

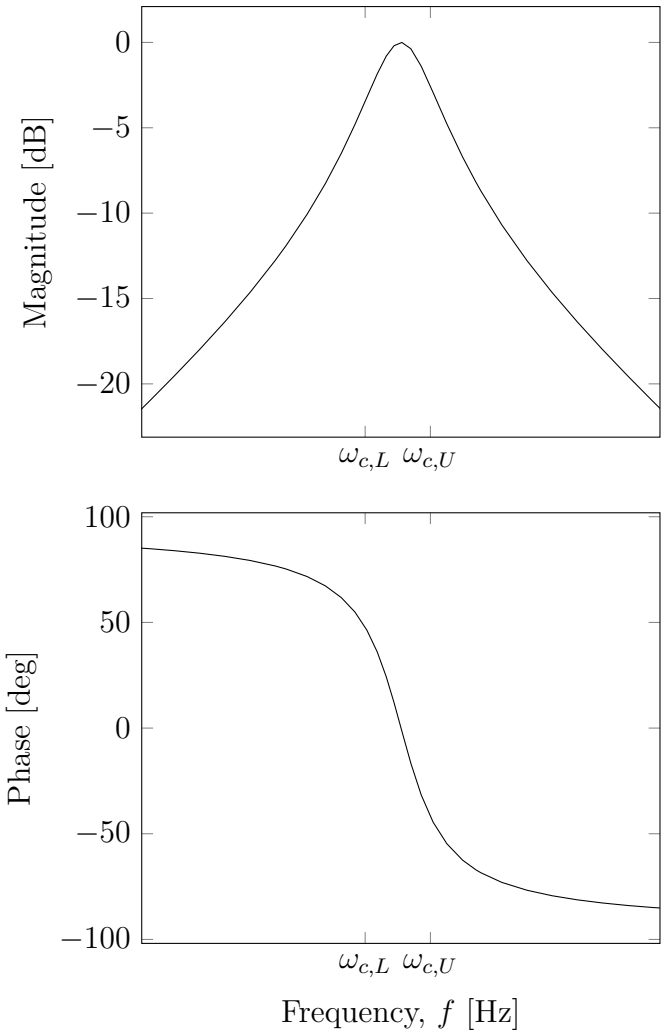

Fig. 3.1. Bode diagram showing the magnitude gain and phase shift of the BPF.

3.1.1 Setup

The BPF is implemented in Simulink according to (3.1) - (3.2) and with the parameters presented in Table 3.1.

Table 3.1: Parameters used in the band-pass filter for signal estimation.

Parameter	Description	Value	Unit
ω_0	Center frequency	$2\pi 10$	[rad/s]
$\omega_{c,L}$	Lower cutoff frequency	$2\pi 8$	[rad/s]
$\omega_{c,U}$	Upper cutoff frequency	$2\pi 12$	[rad/s]

3.2 Phase-locked loop

A phase-locked loop (PLL) is a feedback control system that generates an oscillating output signal whose phase is maintained close or locked to that of an input reference signal [9]. There are many successful applications of PLLs such as line synchronisation, colour sub-carrier recovery in TV receivers, FM and PM demodulators in radio receivers, frequency synthesisers in transceivers and signal generators, power grid synchronisation and many more. In [10] typical techniques for monitoring and synchronization using PLL systems were compared and analyzed in terms of accuracy and dynamic response. The benchmarking revealed that the second-order generalized integrator (SOGI) PLL system is a promising solution for monitoring and synchronization in single-phase applications. A block diagram of the SOGI-PLL proposed in [11] can be seen in Fig. 3.2.

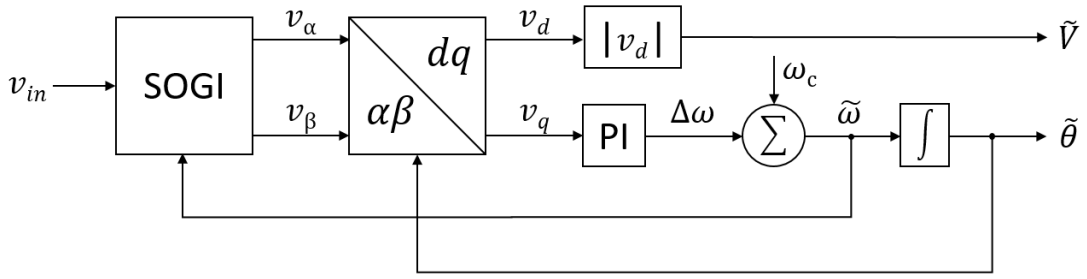

Fig. 3.2. Block diagram including the fundamental building blocks and operations of a SOGI based PLL.

The system input is the reference signal v_{in} with amplitude V, frequency ω and angle $\theta = \omega t + \phi$, where t is the time and ϕ is the phase. The system outputs are the estimated amplitude $\tilde{V}$ and angle $\tilde{\theta}$. The implementation of the SOGI block can be seen in Fig. 3.3 and the corresponding characteristic transfer functions are

$$G_\alpha(s) = \frac{v_\alpha(s)}{v_{in}(s)} = \frac{k_{SOGI}\tilde{\omega}s}{s^2 + k_{SOGI}\tilde{\omega}s + \tilde{\omega}^2} \tag{3.3}$$

$$G_\beta(s) = \frac{v_\beta(s)}{v_{in}(s)} = \frac{k_{SOGI}\tilde{\omega}^2}{s^2 + k_{SOGI}\tilde{\omega}s + \tilde{\omega}^2} \tag{3.4}$$

where v_α and v_β are a pair of 90° shifted output signals and k_{SOGI} is a constant term referred to as the damping factor, which can be used for regulating the bandwidth and dynamic response of the estimated output signals. $\tilde{\omega}$ is the estimated frequency.

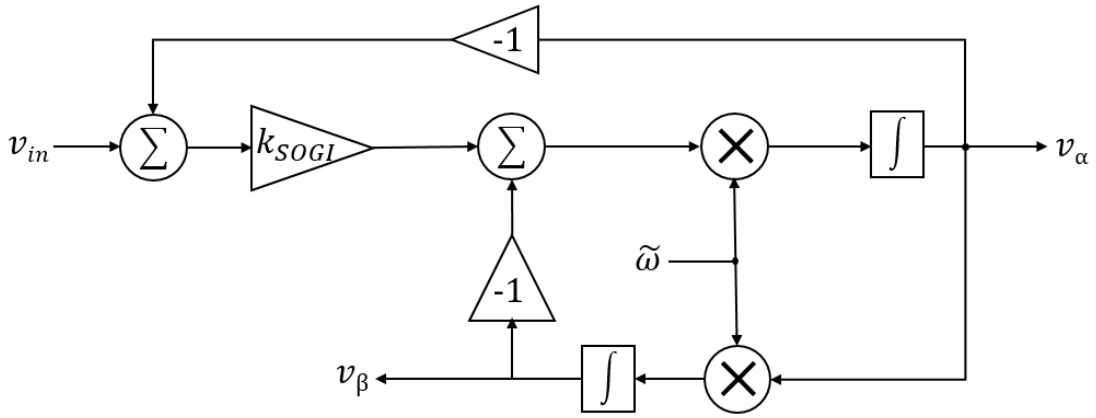

Fig. 3.3. Block diagram of the SOGI used for phase detection in the PLL seen in Fig. 3.2.

Following the SOGI block is the Park transformation ($\alpha\beta \rightarrow dq$) which gives the estimated input signal amplitude v_d, and the phase error signal v_q as

$$\begin{aligned} v_d &= cos(\tilde{\theta})v_\alpha + sin(\tilde{\theta})v_\beta, \\ v_q &= -sin(\tilde{\theta})v_\alpha + cos(\tilde{\theta})v_\beta \end{aligned} \tag{3.5}$$

In order to attenuate high-frequency noise and achieve a fast transient response v_q is passed through a proportional-integral (PI) controller with transfer function

$$F_{PI}(s) = \frac{k_{pll}s + k_i}{s} \tag{3.6}$$

where k_{pll} is the proportional gain and k_i is the integral gain. The center frequency ω_c is then added to the control output signal $\Delta\omega$ in order to reduce control effort and accelerate the lock-in process. The resulting frequency estimate, $\tilde{\omega}$, is finally integrated to generate the estimated angle $\tilde{\theta}$. For a detailed mathematical analysis of the SOGI-PLL, see [12].

3.2.1 Setup

A SOGI-PLL is modeled in Simulink to allow for performance analysis of signal tracking in regards to speed and accuracy. To retrieve the oscillatory component (in the region of ω_c) of the signal without any offset, the PLL method for signal estimation incorporates a pre-filter for the input signal. A desirable behaviour is achieved when using a high-pass filter (HPF) with a cutoff frequency at 20% of the center frequency according to

$$H_{hp}(s) = \frac{0.2\omega_c s}{0.2\omega_c s + (0.2\omega_c)^2} \tag{3.7}$$

By analysing the relationship of the settling time and overshoot of (3.3) - (3.4) an optimal value for the damping factor k_{SOGI} in the SOGI-block is found as in (3.8).

$$k_{SOGI} = \frac{1}{\sqrt{2}} \tag{3.8}$$

Similarly the PI-control gains in (3.6) are chosen with speed and accuracy in mind. The complete list of parameters used for the analysis of the SOGI-PLL are presented in Table 3.2.

Table 3.2: Parameters used in the SOGI-PLL system for signal estimation.

Parameter	Description	Value	Unit
ω_c	Center frequency	$2\pi 10$	[rad/s]
k_{SOGI}	SOGI damping factor	$\frac{1}{\sqrt{2}}$	[-]
k_i	Integral gain	$0.2\omega_c$	[-]
k_{pll}	Proportional gain	$0.2\omega_c$	[-]

3.3 Discrete Fourier transform

The Discrete Fourier transform (DFT) is widely used in signal processing applications. It transforms a signal from time domain to frequency domain making it possible to decompose signals into several sine waves. In [13] the DFT is defined as

$$F[k] = \sum_{n=0}^{N-1} x[n] e^{-\frac{i2\pi kn}{N}}, \quad k \in [0, N-1] \tag{3.9}$$

where x is the sampled signal in the time domain with length N, and where F is the Fourier transform of x. F results in a vector, also with length N, with complex numbers that can be used to calculate the phase and magnitude of the signal at different frequencies. With these, it is possible to recreate the signal with only selected frequencies.

The phase Φ for the desired frequency, can be calculated as

$$\Phi = tan^{-1}(\mathrm{Im}(F[k]), \mathrm{Re}(F[k])) \tag{3.10}$$

The amplitude A_{osc} can be computed according to

$$A_{osc} = \frac{1}{N}\sqrt{\mathrm{Re}(F[k])^2 + \mathrm{Im}(F[k])^2} \tag{3.11}$$

The oscillation part of the signal P_{osc} can then be recreated as

$$P_{osc} = A_{osc}\cos(f_0 2\pi t + \Phi) \tag{3.12}$$

where f_0 is the known frequency of the signal to be estimated.

The relationship between the index k in F and a signal with frequency f_0 sampled at the rate f_s can be described by (3.13).

$$k = \frac{f_0 N}{f_s} \tag{3.13}$$

The frequency resolution Δf of the DFT can be calculated with

$$\Delta f = \frac{f_s}{N} \tag{3.14}$$

and to get a good result of the DFT, it is beneficial if f_0 is evenly divisible by Δf.

3.3.1 Setup

The Fast Fourier transform (FFT) is a fast and efficient algorithm for calculating the DFT, and is easily done in MATLAB with the fft command.

In each time step the FFT can be calculated using the last N samples of the signal. The signal can then be reconstructed using (3.10) - (3.12). The parameters used are presented in Table 3.3.

Table 3.3: Parameters used in the DFT signal estimation.

Parameter	Description	Value	Unit
f_0	Frequency to estimate	10	[Hz]
f_s	Sampling rate	1000	[Hz]
N	Number of samples	200	[-]

3.4 Recursive least squares filter

The Recursive Least Squares (RLS) method is an adaptive filter algorithm used to estimate signals based on a given model of the investigated system. It does so by recursively selecting the filter coefficients that minimizes a linear least squares cost function related to the input signal. In [14] a novel method for increasing the dynamic performance of an RLS algorithm for fast estimation of low-frequency oscillations in power systems is proposed. Here the input power signal $p(t)$ is modeled as the sum of an average and an oscillatory term $P_{avg}(t)$ and $P_{osc}(t)$ respectively according to

$$p(t) = P_{avg}(t) + P_{osc}(t) \tag{3.15}$$

where the oscillatory component $P_{osc}(t)$ can be expressed in terms of its amplitude $A_{osc}(t)$, oscillation frequency ω_{osc} and phase $\phi(t)$ as

$$P_{osc}(t) = A_{osc}(t)cos(\omega_{osc}t + \phi(t)) \tag{3.16}$$

giving

$$p(t) = P_{avg}(t) + A_{osc}(t)cos(\theta_{osc}(t) + \phi(t)) \tag{3.17}$$

where $\theta_{osc}(t) = \omega_{osc}t$ is the oscillation angle. Now consider a discrete generic input signal $y(k)$ as the sum of its estimate $\tilde{y}(k)$ and estimation error $d(k)$ as

$$y(k) = \tilde{y}(k) + d(k) = \Phi(k)\tilde{h}(k-1) + d(k) \tag{3.18}$$

where Φ(k) is the model dependent observation matrix, and can be expressed as

$$\Phi(k) = \begin{bmatrix} 1 \\ cos(\theta_{osc}(k)) \\ -sin(\theta_{osc}(k)) \end{bmatrix} \tag{3.19}$$

for low-frequency oscillations. The estimated state vector $\tilde{h}(k)$ is updated recursively in the RLS algorithm according to

$$\tilde{h}(k) = \tilde{h}(k-1) + G(k)[y(k) - \Phi(k)\tilde{h}(k-1)] \tag{3.20}$$

where $G(k)$ is the gain matrix given by

$$G(k) = \frac{R(k-1)\Phi^{\top}(k)}{\lambda + \Phi(k)R(k-1)\Phi^{\top}(k)} \tag{3.21}$$

Here $R(k)$ is the covariance matrix which is updated recursively as

$$R(k) = [I - G(k)\Phi(k)]\frac{R(k-1)}{\lambda}, \quad 0 < \lambda \leq 1 \tag{3.22}$$

where λ is the forgetting factor and I is the identity matrix.

The signal $p(t)$ according to (3.17) can be expressed as

$$p(t) = P_{avg}(t) + P_d cos(\theta(t)) - P_q sin(\theta(t)) \tag{3.23}$$

where

$$\begin{aligned} P_d &= A_{osc}(t)cos(\phi), \\ P_q &= A_{osc}(t)sin(\phi) \end{aligned} \tag{3.24}$$

The signal estimates are obtained from the estimated state vector $\tilde{h}(k)$ as

$$\tilde{h}(k) = \begin{bmatrix} \tilde{P}_{avg}(k) \\ \tilde{P}_d(k) \\ \tilde{P}_q(k) \end{bmatrix} \tag{3.25}$$

and the estimated oscillatory component $\tilde{P}_{osc}$ is calculated according to

$$\tilde{P}_{osc} = \tilde{A}_{osc}cos(\theta_{osc}(k) + \tilde{\phi}(k)) \tag{3.26}$$

where the estimated amplitude $\tilde{A}_{osc}$ of the oscillation component is obtained by

$$\tilde{A}_{osc} = \sqrt{\left(\tilde{P}_d(k)\right)^2 + \left(\tilde{P}_q(k)\right)^2} \tag{3.27}$$

and the estimated phase $\tilde{\phi}(k)$ is found as

$$\tilde{\phi}(k) = tan^{-1}\left(\frac{\tilde{P}_q(k)}{\tilde{P}_d(k)}\right) \tag{3.28}$$

3.4.1 Varying forgetting factor

As shown by (3.18) - (3.22) the algorithm is performed recursively, starting from an initial invertible matrix $R(0)$ $(= I)$ and initial state vector $\tilde{h}(0)$ $(= [0\,0\,0]^\top)$ [15]. The cost function, $\xi(k)$, that the RLS algorithm minimizes is

$$\xi(k) = \sum_{n=0}^{k} |d(n)|^2 \lambda^{k-n} \tag{3.29}$$

In steady state, the estimation speed for the algorithm is found as

$$\alpha_{RLS} = \frac{1-\lambda}{t_s} \tag{3.30}$$

where α_{RLS} is the bandwidth of the estimator and t_s is the sampling time. As can be observed from (3.30) the bandwidth of the RLS algorithm is directly dependent on the forgetting factor λ. A large forgetting factor yields a low estimation speed and high frequency selectivity whereas a lower value gives a higher estimation speed and lower frequency selectivity. A desirable behaviour is to have a fast estimation speed during rapid changes in the input signal, while still having a high frequency selectivity. This is achieved by varying λ between two predefined values in a controlled manner, according to Fig.3.4.

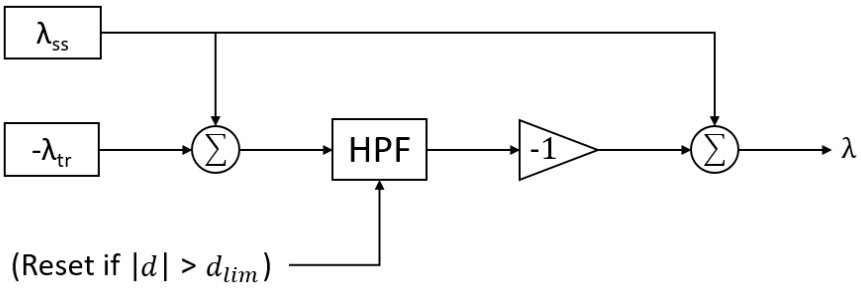

Fig. 3.4. Block diagram for varying the forgetting factor λ between its steady state value, λ_{ss}, and its transient value, λ_{tr}, by resetting a HPF if the error, d, exceeds a predetermined limit, d_{lim}.

If the algorithm detects a rapid change in the input signal (i.e. the absolute value of the error $d(k)$ exceeds some predefined limit d_{lim}), λ is lowered from its steady state value, λ_{ss}, to its transient value, λ_{tr}. To guarantee the frequency selectivity of the RLS algorithm λ is then increased back to its steady state value in the fashion of the step response of a HPF, see Fig. 3.5.

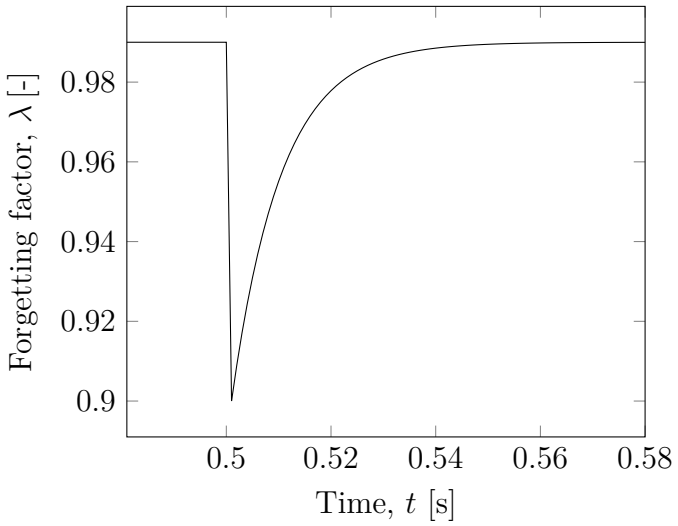

Fig. 3.5. Visualization of λ as the difference ($d(k)$) between the true signal $y(t)$ and the estimated signal $\tilde{y}(t)$ exceeds the predefined error limit d_{lim} and thereby triggers the HPF to reset at $t = 0.5\,\text{s}$.

In the example shown in Fig. 3.5 the explained characteristics for λ can be seen when $d(k) > d_{lim}$ at $t = 0.5\,\text{s}$. In the example $\lambda_{ss} = 0.99$ and $\lambda_{tr} = 0.9$. These values and the design of the HPF should be carefully considered and tuned to achieve the behaviour desired for the intended application. By implementing the estimator with a variable forgetting factor the RLS algorithm is able to quickly separate the two signal components accurately in the presence of disturbances [16].

3.4.2 Frequency adaptation

The performance of the RLS algorithm in steady state is dependent on the parameters in the observation matrix Φ which contains information about the signal according to (3.18) and (3.19). Here θ_{osc} is integrated from the initially assumed oscillation frequency ω_{osc0}. If the frequency of the oscillating component changes the model should be updated correspondingly [16]. This can be achieved by utilizing a frequency adaptation mechanism according to Fig. 3.6.

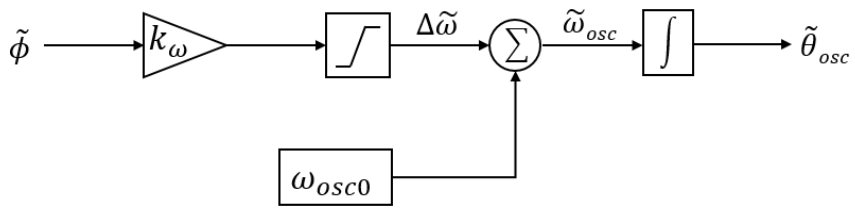

Fig. 3.6. Block diagram of frequency estimator used with the RLS algorithm.

In Fig. 3.6 the oscillation frequency is estimated according to

$$\tilde{\omega}_{osc} = \omega_{osc0} + \Delta\tilde{\omega}\,, \quad \Delta\omega_{min} \leq \Delta\tilde{\omega} \leq \Delta\omega_{max} \tag{3.31}$$

where $\tilde{\omega}_{osc}$ is the estimated oscillation frequency and $\Delta\tilde{\omega}$ is the limited frequency change according to

$$\Delta\tilde{\omega} = k_\omega\tilde{\phi} \tag{3.32}$$

where k_ω is the gain of the frequency estimator. $\Delta\omega_{min}$ and $\Delta\omega_{max}$ are the upper and lower limits for the changes in oscillation frequency to track. The phase estimate $\tilde{\phi}$ is given by (3.28).

3.4.3 Setup

An RLS algorithm with variable forgetting factor and a frequency adaptation method is assembled as in Fig. 3.7.

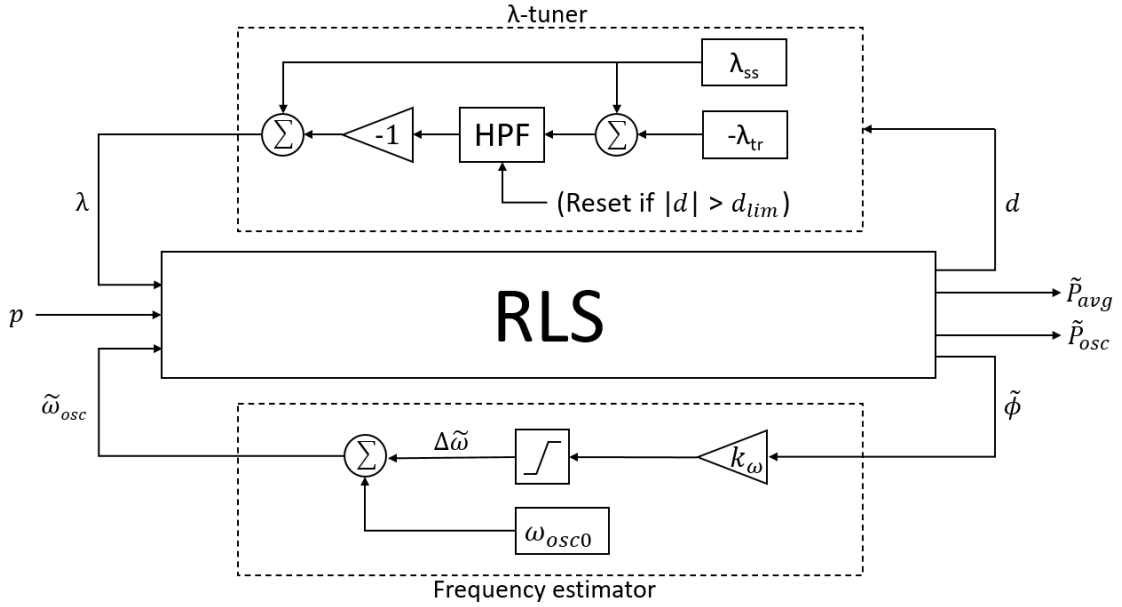

Fig. 3.7. Block diagram of λ-tuner and frequency estimator used with the RLS algorithm for separating a signal p into an estimated average term, $\tilde{P}_{avg}$, and an estimated oscillating term, $\tilde{P}_{osc}$.

By implementing the RLS algorithm in Simulink it can be analysed and compared to the other methods. The values chosen for the parameters determining the behaviour of the RLS algorithm are presented in Table 3.4.

Table 3.4: Parameters used in the RLS algorithm for signal estimation.

Parameter	Description	Value	Unit
$\Delta\omega_{max}$	Upper limit for frequency change	$2\pi 2$	[rad/s]
$\Delta\omega_{min}$	Lower limit for frequency change	$-2\pi 2$	[rad/s]
λ_{ss}	Steady state forgetting factor	0.999	[-]
λ_{tr}	Transient forgetting factor	0.97	[-]
ω_{osc0}	Initially assumed oscillation frequency	$2\pi 10$	[rad/s]
d_{lim}	Error limit for lowering λ	1	[-]
k_ω	Frequency estimator gain	$0.2\omega_{osc0}$	[-]
t_s	Sampling time for the RLS algorithm	0.001	[s]

3.5 Analysis

To choose the filtering technique best suited for retrieving the oscillations in the range of the eigenfrequency of the drivetrain, the different methods described in chapter 3.1 - 3.4 are tested and their performance is compared for different cases. The properties considered to be most important for the estimation methods are: settling time, frequency selectivity and phase and amplitude accuracy.

3.5.1 10 Hz tracking

In order to compare settling time and phase accuracy, a sine wave with frequency 10 Hz and amplitude 10, as seen in Fig. 3.8, is filtered using the four methods.

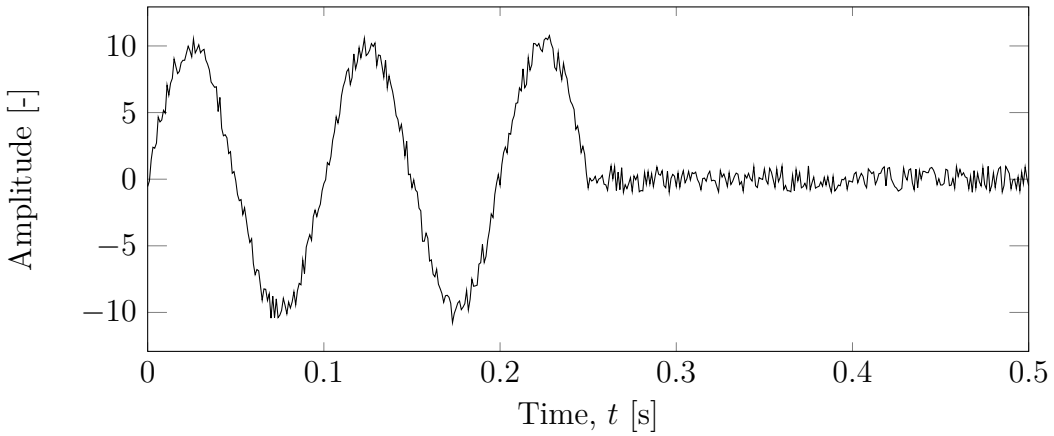

Fig. 3.8. Input to the signal estimation techniques, an oscillation with amplitude 10 at frequency 10 Hz, with added random noise of amplitude 1 and frequency 250 Hz.

Random noise with amplitude 1 and frequency 250 Hz (this is the frequency at which the noise is most powerful in the EM speed measurement) is added to review the different filters ability to attenuate measurement noise. The results are shown in Fig. 3.9. The continuous black line is the reference, i.e. the input signal seen in Fig. 3.8 but without noise, and the dashed lines are the outputs from the filters.

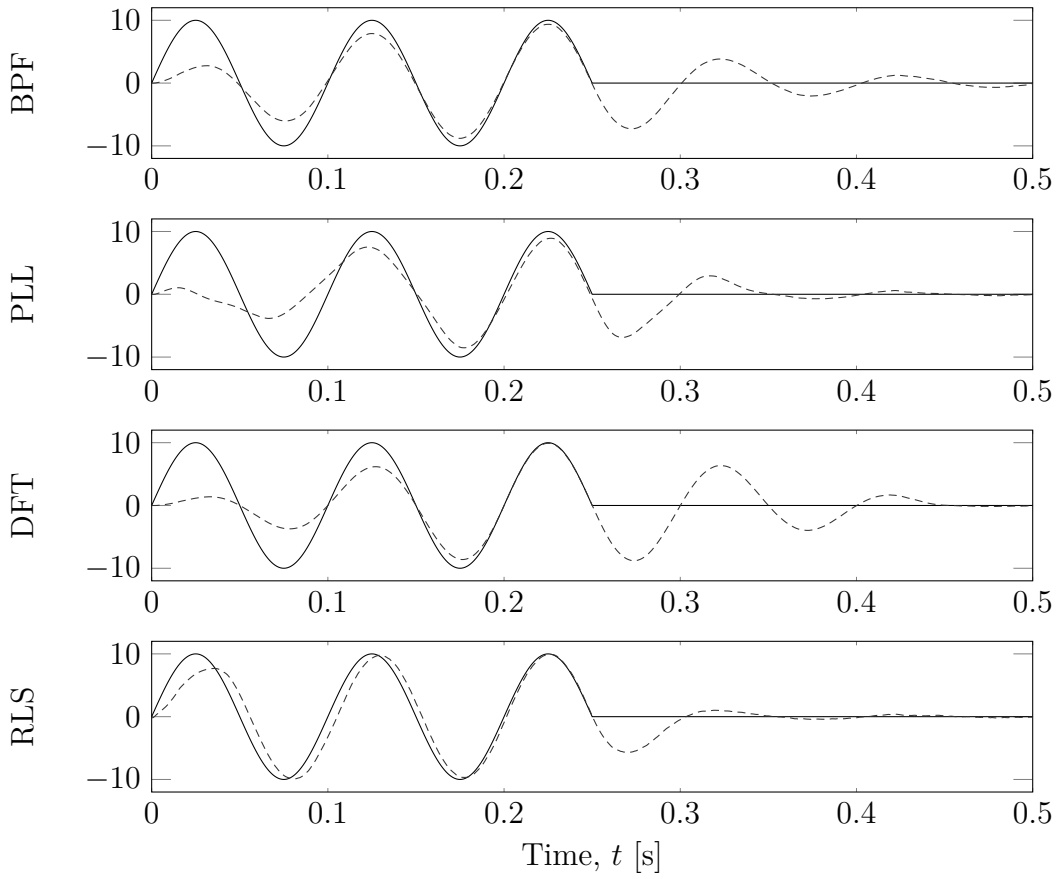

Fig. 3.9. Tracking of the noisy 10 Hz signal seen in Fig. 3.8. The continuous line is the reference and the dashed lines are the different filter outputs.

As can be seen in Fig. 3.9 the RLS filter seems to find the correct amplitude after less than one period, and the correct phase after about two periods. The BPF seems to find the phase after less than a period while lacking in amplitude. The DFT behaves similar to the BPF but is a bit slower at gaining amplitude. The PLL does not seem to fully lock on the reference. As the reference signal suddenly stops oscillating at $t = 0.25\,\mathrm{s}$ the RLS is the fastest at settling, followed by the PLL, DFT and finally the BPF who keep oscillating for some periods.

Both properties of amplitude and frequency accuracy are important and based on this result alone it is not possible to determine the most suitable method, however, for this case the RLS seems to generate the most promising result. All of the filters are excellent at attenuating the high frequency noise.

3.5.2 Oscillating ramp

As mentioned, an important property of the signal estimation technique is frequency selectivity. It should be able to reject leakage from an average component, and low frequency signals should be attenuated while the oscillating part is let through. This is of importance as an oscillation in reality could occur at a positive speed and

during an acceleration or retardation. The different methods' abilities to attenuate low frequencies are tested by filtering a signal with a steep ramp and an added sine wave, as seen in Fig. 3.10.

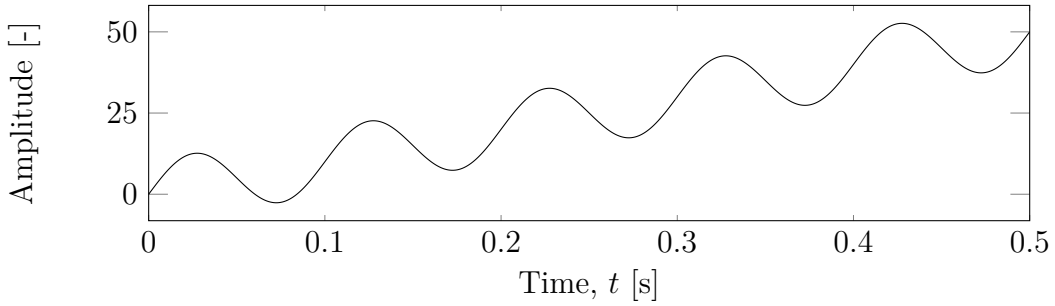

Fig. 3.10. Input to the signal estimation techniques, a ramp with an added oscillation at frequency 10 Hz.

The average component of the signal in Fig. 3.10 goes from 0 to 50 while the oscillations are of amplitude 10 and frequency 10 Hz. The results from the different filtering methods are presented in Fig. 3.11.

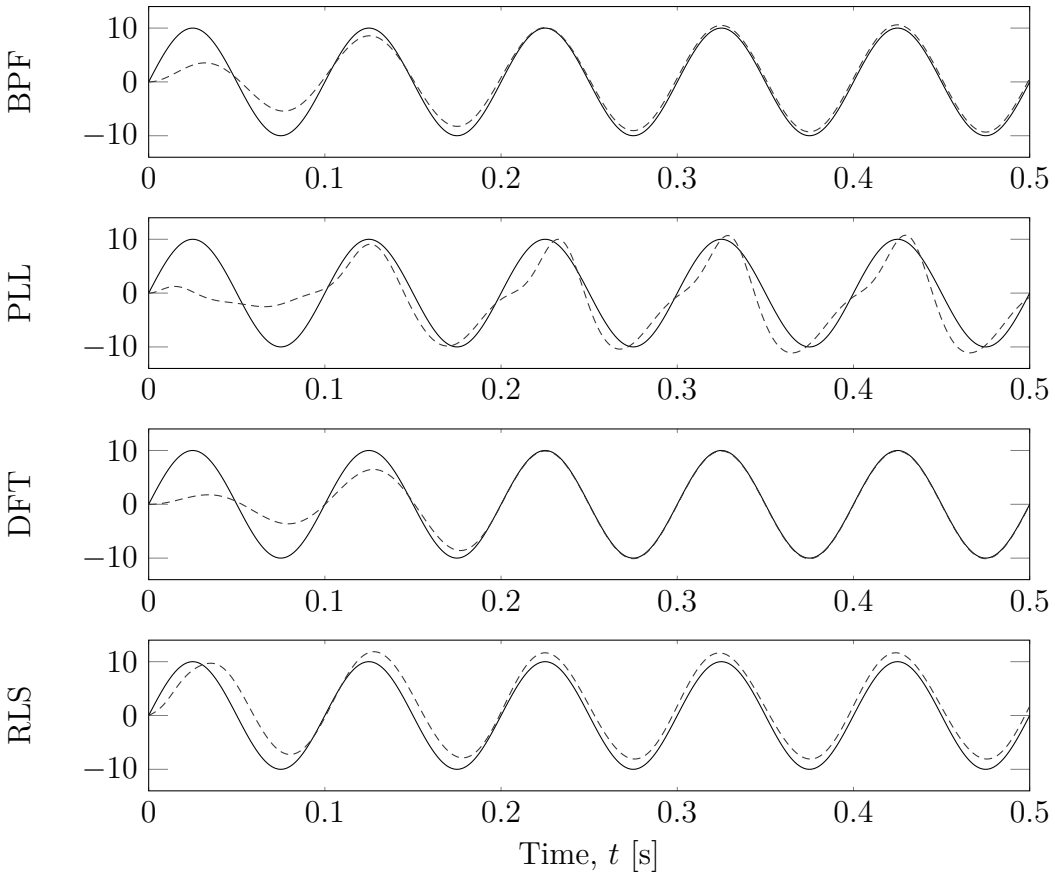

Fig. 3.11. The four estimation techniques filtering the 10 Hz signal with a steep ramp that can be seen in Fig. 3.10. The continuous line is the reference and the dashed lines are the outputs from the different methods.

As can be seen in Fig. 3.11, the DFT handles the ramp without any leakage from the average component, but again is slow at gaining in amplitude. The BPF has a small and almost negligible offset owing to the ramp, but is also considered somewhat slow at building up amplitude. The RLS has a small but constant offset from the reference, while gaining amplitude rapidly. The PLL is not able to generate a clean signal. The DFT and BPF are considered to show the most promising performance in regards to eliminating an average component.

3.5.3 Varying frequency

As the investigated system has a varying natural frequency, it is of importance that the signal estimation technique can track a signal as the frequency changes. To investigate how the signal estimation techniques handle this, a sine wave with a frequency sweeping continuously from 8 Hz at $t = 1$ s to 12 Hz at $t = 1.5$ s is filtered and the results are presented in Fig. 3.12.

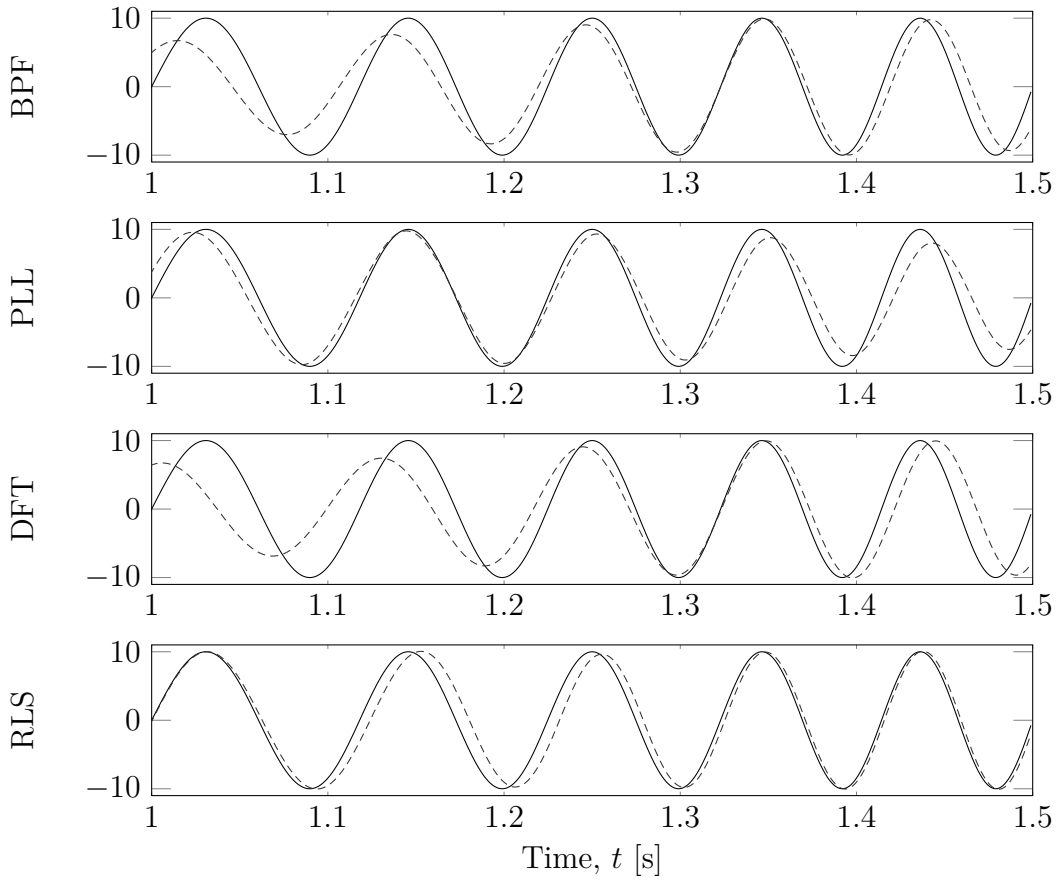

Fig. 3.12. Tracking a signal that changes frequency from $8 - 12$ Hz. The estimation techniques have already settled to 8 Hz at $t = 1$ s. The continuous line is the reference signal and the dashed lines are the different filtering methods' results.

From Fig. 3.12 it is beheld that the RLS is very competent at handling a signal with varying frequency, tracking both amplitude and frequency accurately. The PLL is also performing well but it seems to struggle as the frequency exceeds 11 Hz. The

BPF and DFT lack in both amplitude and frequency precision for lower and higher frequencies.

3.6 Summary

Four different signal estimation methods have been investigated and compared in terms of settling time, frequency selectivity and phase and amplitude accuracy. It has been shown that all methods have different strengths and weaknesses and no single strategy has the best or worst performance for all cases. The PLL has an average performance for all of the cases but does not stand out in any of them. The DFT and BPF show the most promising capability in terms of completely filtering out a low frequency term or average component, however this does not make up for what they lack in terms of gaining amplitude quickly and tracking frequencies in the interval of $8-12\,\mathrm{Hz}$. When it comes to quickly gaining amplitude and following a signal with varying frequency, the RLS shows the most promising results and is ultimately considered to be the best overall signal estimation method for the intended application.

4
Controlled system

Several control strategies with varying levels of complexity have been implemented in combination with the RLS algorithm according to chapter 3.4 and tested together with the plant model presented in chapter 2. In this chapter the two control strategies that show the most promising results in terms of performance and robustness are introduced and studied. Furthermore, a strategy for activating and deactivating the controller is proposed and finally the closed loop behaviour for the entire system according to Fig. 4.1 is analysed through simulations in Simulink.

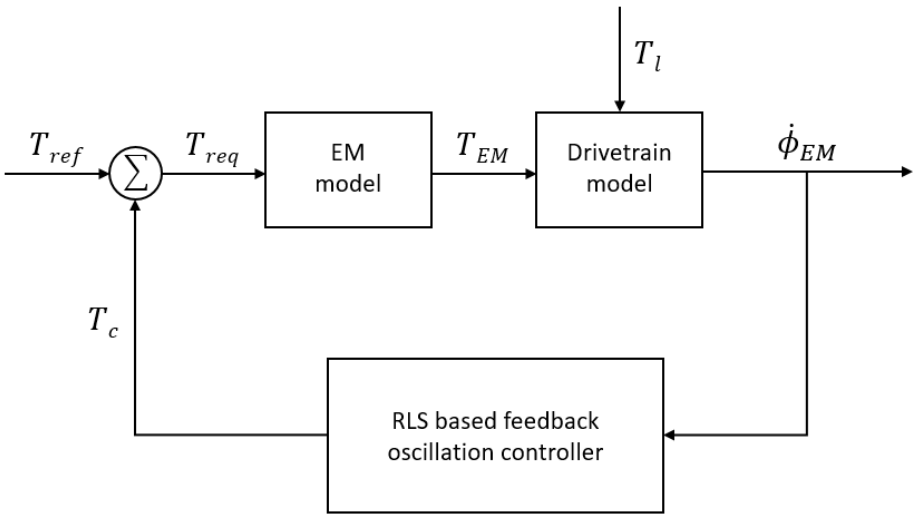

Fig. 4.1. Schematic overview of the investigated system including models of the EM and drivetrain (according to chapter 2) together with an RLS based feedback controller.

4.1 Controller synthesis

The aim of the controller is to calculate a torque, T_c, that when realised by the EM should attenuate the oscillations in the frequency range close to the eigenfrequency of the drivetrain ($8-12\,\text{Hz}$). Properties shared between the controllers include them being based upon the RLS algorithm described in chapter 3.4.

Furthermore, integral action might not be necessary in the controllers as the driver close an outer loop and this introduces some integral action [17]. The control strate-

gies rely on the measured angular velocity of the EM as their input signal and they all use the EM as an actuator for the control signal.

As mentioned in chapter 1.4, the EM is assumed to deliver the requested torque to the drivetrain with ratio 1:1, although with some time delay, t_d. This means that the transfer function representing the *EM model* block in Fig. 4.1, from T_{req} to T_{EM}, can be expressed as a pure time delay according to

$$G_{EM}(s) = e^{-s\,t_d} \tag{4.1}$$

The next block in Fig. 4.1, namely the *Drivetrain model* block, is shown in greater detail in Fig. 4.2 and the corresponding transfer functions are implemented according to chapter 2, in particular from (2.11).

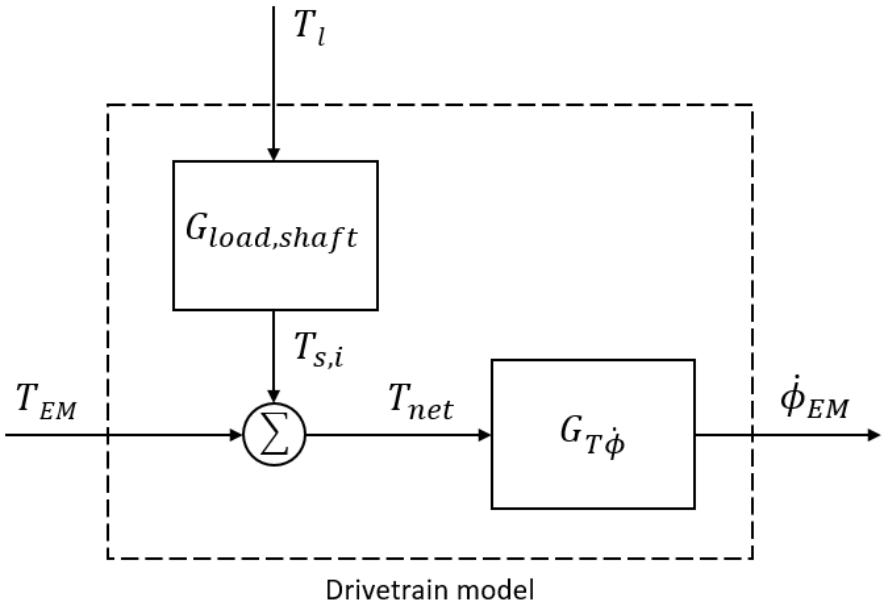

Fig. 4.2. *Drivetrain model* block from Fig. 4.1 with internal transfer functions from EM torque, T_{EM}, and load torque, T_l, to net torque in the shaft, T_{net}, and from the net torque to the EM speed, $\dot{\phi}_{EM}$. The load torque T_l is considered to be an uncontrollable disturbance input acting on the drivetrain, and the EM torque, T_{EM} is a controllable input.

The transfer function from the external load torque disturbance, T_l, to the shaft torque, $T_{s,i}$, is

$$G_{load,shaft}(s) = -\frac{c_s\,s + k_s}{i_d\,(J_l\,s^2 + c_s\,s + k_s)} \tag{4.2}$$

and the transfer function from the net torque in the shaft, T_{net}, to the angular velocity at the EM, $\dot{\phi}_{EM}$, is found as

$$G_{T\dot{\phi}}(s) = \frac{J_l\,s^2 + c_s\,s + k_s}{J_{\mathrm{EM}}\,J_l\,s^3 + c_s\,(J_{\mathrm{EM}} + \frac{J_l}{i_d^2})\,s^2 + k_s\,(J_{EM} + \frac{J_l}{i_d^2})\,s} \tag{4.3}$$

Another property shared for the controller implementation is a supervisory logic, according to chapter 4.2, for switching the controller on and off.

4.1.1 Proportional gain controller

In [18] it has been shown that power oscillation damping can be successfully achieved by using an RLS algorithm in combination with a pure proportional gain controller (P controller). A possible benefit of having a controller that is completely independent of the plant model, compared to a model based approach, is that it could be less sensitive to errors or changes in the model parameters. It also requires minimal computation effort and is easy to tune as it only contains one tuning parameter [19]. In Fig. 4.3 a block diagram for the estimation based proportional gain controller is shown.

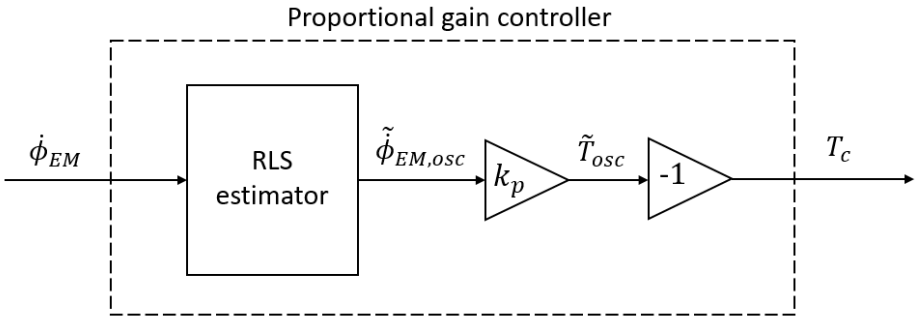

Fig. 4.3. Block diagram for the estimation based proportional gain controller.

The corresponding transfer function is

$$K_P(s) = -k_p\, G_{RLS}(s) \tag{4.4}$$

where k_p is the proportional gain constant in Nms/rad that translates the estimated oscillation speed, $\tilde{\dot{\phi}}_{EM,osc}$, into the estimated torque oscillation $\tilde{T}_{osc}$ [2]. $G_{RLS}(s)$ is the transfer function of the RLS estimator according to chapter 3.4. After the estimated oscillatory component of the angular velocity at the EM is multiplied by k_p it is fed back to the actuator with negative sign as T_c to compensate for the torque oscillations, and this controller therefore targets at completely removing the oscillations in the EM speed.

The level of attenuation is determined by the control gain k_p, where a higher value achieves greater oscillation rejection at the price of more aggressive actuation and reduced robustness. The controller is tuned in an iterative manner in order to achieve a good compromise between oscillation attenuation and robustness, and the chosen value is presented in Table 4.1 in chapter 4.3.

4.1.2 Linear-quadratic-Gaussian controller

A common control technique for linear systems is the Linear-quadratic-Gaussian controller (LQG). It consists of two parts, where the first is a Linear-quadratic regulator (LQR) and the second is a Kalman filter, also know as a Linear-quadratic estimator (LQE). The Kalman filter is used to estimate the states of the system.

By using the LQG it is possible to give a torque control input to compensate for all states rather than only the oscillations in the EM speed measurement. This could potentially yield a better result than the P controller as it is the ultimate goal to damp the oscillations in the drive shaft rather than the oscillations in the EM speed. A possible downside, if compared to the P controller, is that it requires a model of the plant, and hence it is not as versatile and easy to implement. It also requires more real-time computation [5] and might be less robust to variations in the plant.

4.1.2.1 Linear-quadratic regulator

The LQR is a full state feedback controller that finds the optimal pole positions of a feedback system. In [20] this is done by minimizing the cost function

$$J = \int_0^\infty x^T Q x + u^T R u \, dt \tag{4.5}$$

and results in a feedback controller of the form

$$u = -k_{LQR} x \tag{4.6}$$

where k_{LQR} is the LQR gain vector that is calculated from

$$k_{LQR} = R^{-1} B^T P \tag{4.7}$$

where P is found by solving the Riccati equation according to

$$A^T P + PA - PBR^{-1}B^T P + Q = 0 \tag{4.8}$$

Here Q and R are weight matrices used for penalizing state differences and control signals.

The relationship between Q and R determines the behaviour of the controller. A low value for R and a high value for Q results in a controller that uses the control signal a lot while trying to keep the states as close to zero as possible. However, if the value of R is set high, the control signal is considered expensive and results in a slower controller that utilizes the control signal less.

In this work a fast controller is important and it is of great importance that the states are kept low. It is especially important that the torsion is kept low. Tuning accordingly resulted in the following weight matrices

$$Q = \begin{bmatrix} 50 & 0 & 0 \\ 0 & 2 & 0 \\ 0 & 0 & 2 \end{bmatrix}, \quad R = 0.1 \tag{4.9}$$

4.1.2.2 Kalman filter

The LQR is a full state feedback controller, however, in most cases it is not possible to measure all states in a system. A Kalman filter can be used to estimate the states that are not measurable. The system can be described as

$$\begin{aligned} \dot{x} &= Ax + Bu + Gw \\ y &= Cx + v \end{aligned} \tag{4.10}$$

where w is white process noise and v is the white measurement noise with covariance data

$$\mathrm{E}(ww') = Q \quad \text{and} \quad \mathrm{E}(vv') = R \tag{4.11}$$

In the investigated system the disturbance mainly comes from the wheel, causing the angular velocity of the wheel to change. Therefore, the G matrix is set to affect only state x_3, resulting in $G = [001]^\top$.

According to [20] the states can be estimated with

$$\dot{\tilde{x}}(t) = A\tilde{x}(t) + Bu(t) + k_K(y(t) - C\tilde{x}(t)) \tag{4.12}$$

where

$$k_K = PC^T R^{-1} \tag{4.13}$$

and P can be by found solving the Riccati equation

$$AP + PA^T - PC^T R^{-1} P^T C + GQG^T = 0 \tag{4.14}$$

The measurement of the EM angular velocity is considered to have low influence from disturbance compared to the process noise, and thus the covariance data is selected as

$$R = 0.01, \quad Q = 1 \tag{4.15}$$

4.1.2.3 Setup

The gains k_K and k_{LQR} are calculated in MATLAB with the commands lqe and lqr, and the values used for implementation are presented in Table 4.1 in chapter 4.3. The LQG controlled system compares the measured angular velocity with the estimated angular velocity. The error is multiplied with the Kalman gain, k_K, and added to the state estimator, which estimates all three states. The estimated states are multiplied with the LQR gain k_{LQR} in order to generate a control input. The LQR controller strives to keep all states at zero. In order to get the controller to only limit the oscillations, the control input is filtered with the RLS algorithm, leading to only the oscillating part being used as a control input. A visualization of the LQG control strategy can be seen in Fig. 4.4.

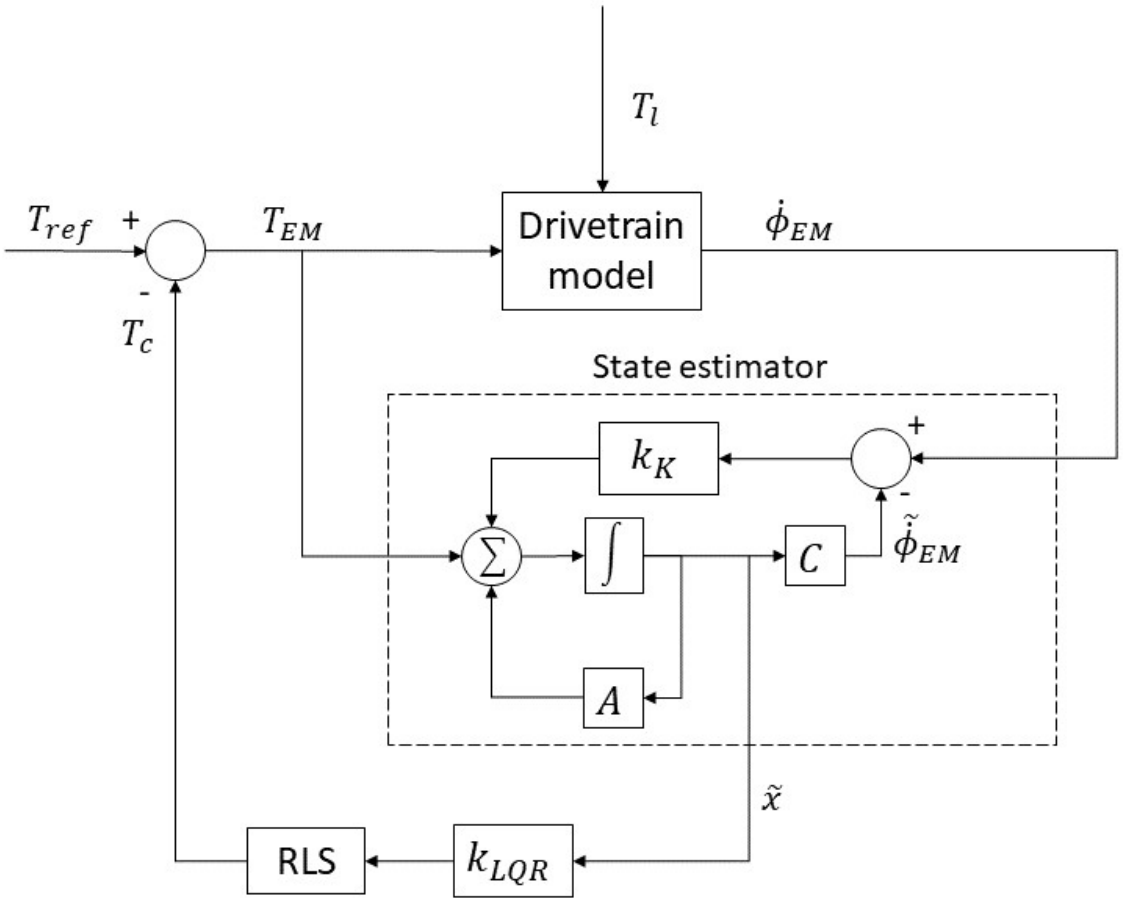

Fig. 4.4. Block diagram of the LQG control strategy.

4.2 Activation logic

The active drivetrain oscillation damper is required in a limited range of scenarios. In order to ensure that the controller does not affect the system in the absence of harmful oscillations, some supervisory logic should be implemented for switching the controller on and off. Different examples of activation logic for anti-jerk controllers are discussed in [3]. Solutions typically involve some predefined threshold for the corrective torque, that when exceeded activates the controller. When the corrective torque falls below the deactivation threshold (that may or may not have the same value as the activation threshold) it is turned off.

In this project the activation logic (AL) is based on an RLS estimator as in section 3.4, but with a fixed bandwidth α_{AL}, and without frequency tracking. This is done to achieve a narrower bandwidth and thereby ensure that the controller is only activated in certain cases that are considered as potentially harmful. If the bandwidth is wider, as in the case with a varying forgetting factor and frequency tracking, the controller is activated too easily, leading to active damping also for oscillations in frequencies outside the critical region, resulting in decreased performance and driveability.

The RLS used in the activation logic takes the measured EM speed, $\dot{\phi}_{EM}$, as input, and outputs the estimated oscillation, $\dot{\phi}_{EM,osc}$. If the amplitude of the estimated oscillation exceeds the activation threshold, A_{th}, the controller is activated. For the controller to be deactivated the amplitude of the oscillations has to lay below the deactivation threshold, D_{th}, for some time t_{AL}. A state machine representing the activation logic can be seen in Fig. 4.5.

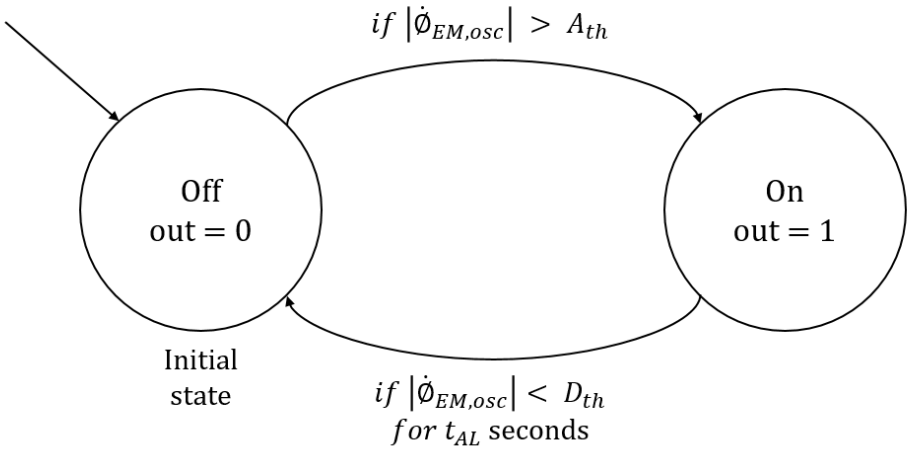

Fig. 4.5. State machine representation of the activation logic for the controller.

As seen in Fig. 4.5 the state machine is initially set to the off state and outputs a value of 0. If the activation condition is fulfilled the state machine will instead output a 1. The output value from the state machine is multiplied by the output from the torque controller to generate the control signal to the actuator.

Careful consideration is taken when choosing the values of A_{th}, D_{th} and t_{AL} as they determine how and when the controller is engaged and disengaged. If for example the value of A_{th} is set too low the controller could be activated during a quick acceleration or retardation, reducing the experienced performance of the car. If the value is set too high the controller might not be engaged early enough to prevent damage to the drive shaft and other possible consequences as discussed in chapter 1. The same reasoning applies when choosing the values for D_{th} and t_{AL} that determine when to disengage the controller. If it is done too late the driveability might be decreased but if it is done too soon the oscillations might still be at concerning levels.

Suitable values are found by analyzing real measurement data of the EM speed in cases when resonance in the drive shafts has been confirmed, such a measurement can be seen in Fig. 2.4 in chapter 2. The chosen values are presented in Table 4.1 in chapter 4.3.

4.3 Full system simulation setup

The proposed controllers, with integrated RLS algorithm and auxiliary activation logic, are connected to the EM and drivetrain models according to Fig. 4.1. The full system is implemented in Simulink with the values presented in Table 4.1.

Table 4.1: Parameters used in the full system simulation setup.

Parameter	Description	Value	Unit
t_d	EM actuation delay	0.003	[s]
k_p	Proportional gain constant	5	[Nms/rad]
k_{LQR}	LQR gain	[-19.6 3.3 10.3]	[-]
k_K	Kalman gain	[-0.11 83.4 9.75]$^\top$	[-]
α_{AL}	RLS bandwidth for AL	1	[rad]
A_{th}	Activation threshold for AL	10	[rad/s]
D_{th}	Deactivation threshold for AL	5	[rad/s]
t_{AL}	Time constant for AL	0.1	[s]

The values that are used for the nominal plant model are the same as the ones used for the analysis of the mechanical drivetrain model in chapter 2.3 and can be seen in Table 2.1. The parameters used for the RLS estimator are unchanged from the analysis of the signal estimation techniques in chapter 3 and can be seen in Table 3.4. Because the EM is only able to supply limited torque the total torque request to the EM, T_{req}, is limited to $\pm 350\,\mathrm{N\,m}$ in the simulations.

4.4 Analysis

In this section the two controllers that have been proposed, the P controller and the LQG controller, are analyzed in terms of performance and robustness. Many different combinations of input signals, T_{EM} and T_l, representing different driving scenarios, have been studied. The ones presented in this section are considered to be significant and to capture the overall behaviour of the system and controllers. Only one factor is changed at a time to enable consequential comparison between the scenarios.

The states used for evaluating the controllers are the EM speed (x_2) and the torsion in the drive shaft (x_1). Factors considered when evaluating the controllers are: response time, peak oscillation attenuation, oscillation attenuation for varying frequency oscillations and robustness to variations in the plant model, i.e. variations in the plant model parameters. Furthermore, it is stated in chapter 1.4 that the controller should interfere minimally under normal circumstances, as it might otherwise reduce the performance and associated driveability of the vehicle. This means that the controllers should react only when there are potentially harmful oscillations in the drive shaft, or in other words, if oscillations in the EM speed reach an amplitude of A_{th} (see Table 4.1) for frequencies in the range of $8-12\,\mathrm{Hz}$, as they are the ones considered to be potentially harmful in this project.

4.4.1 Reconstructed real signal

In order to analyze the controllers' overall behaviour and performance, a complex signal originating from real measurement data is studied. A realistic scenario is reconstructed by decomposing a measurement from a test vehicle, where the torque in the drive shaft was measured. The measured torque from the real case is the result of some unknown EM and load toque acting on the drivetrain. Because the model used for simulation requires two inputs, T_{EM} and T_l, the RLS algorithm is used for splitting the real measurement signal into two parts. The RLS outputs an average and an oscillatory component. The average part is used as the EM torque input, T_{EM}, to the plant, and the oscillatory part is used to simulate a disturbance from the wheel side of the drivetrain, T_l.

The disturbance, T_l, has a varying frequency with a power spectrum similar to the power spectrum presented in Fig. 2.5 in chapter 2, where the power is mainly concentrated around $8-12\,\text{Hz}$. The nominal plant model is used in the simulation, and hence the resonance frequency is $10\,\text{Hz}$. The oscillation reduction that the two controllers achieve for the reconstructed scenario can be seen in Fig. 4.6. The uncontrolled output from the plant model is shown for reference.

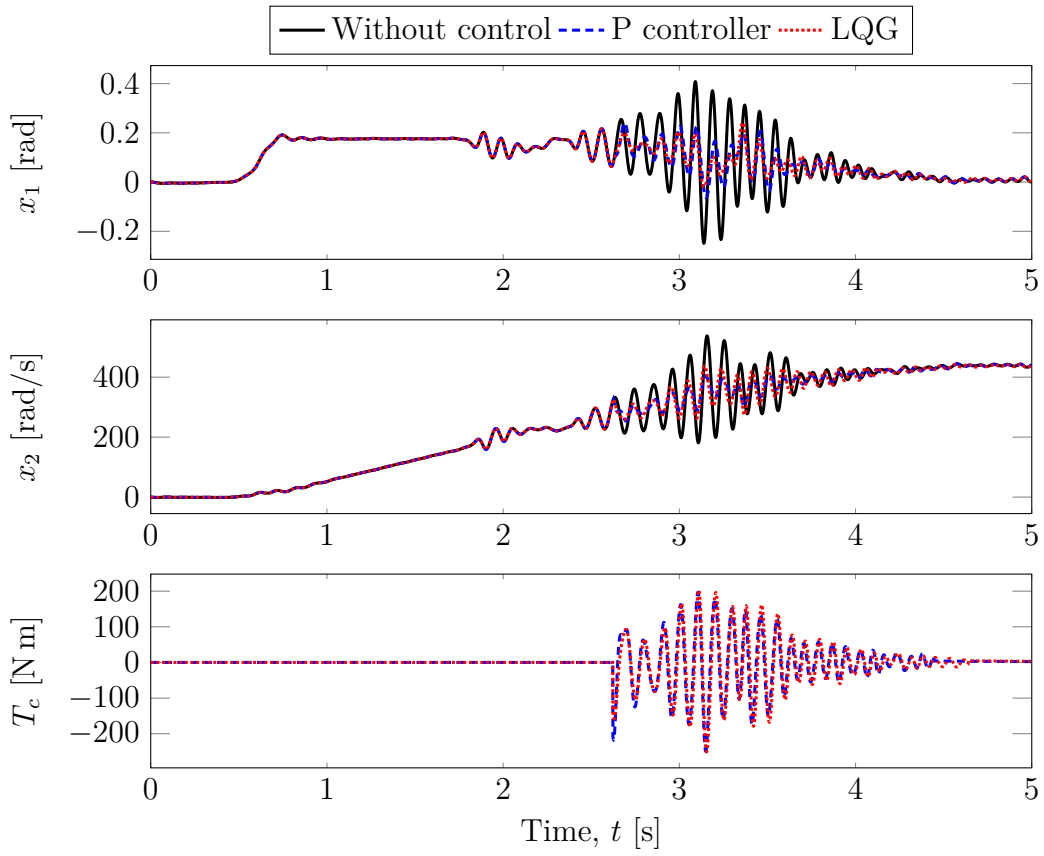

Fig. 4.6. System response when affected by inputs that mimic a real scenario where an oscillating disturbance is applied at the wheel. x_1 is the shaft torsion, x_2 is the angular velocity of the EM and T_c is the torque request from the controller.

The controllers do not change the performance during the acceleration or the end result of the EM angular velocity. Nor do they alter the behavior for oscillations of (in the context) low amplitudes. The driveability and performance is not perceived as decreased at any point, compared to the uncontrolled case. Both controllers seem to have desirable behaviour for the complex scenario, by only engaging during the high amplitude oscillations and disengaging after the amplitudes are decreased sufficiently. As can be seen from the torque request from the controllers (T_c) they do not turn on and off during the high amplitudes, but stay turned on until the oscillations settle.

Both controllers seem to be able to attenuate the oscillations of higher amplitudes that are seen for $t \approx 2.5\,\text{:}4\,\text{s}$. The controllers' performance for the high amplitude oscillations can be seen in greater detail in Fig. 4.7, where the outputs from Fig. 4.6 are highlighted for the mentioned time frame.

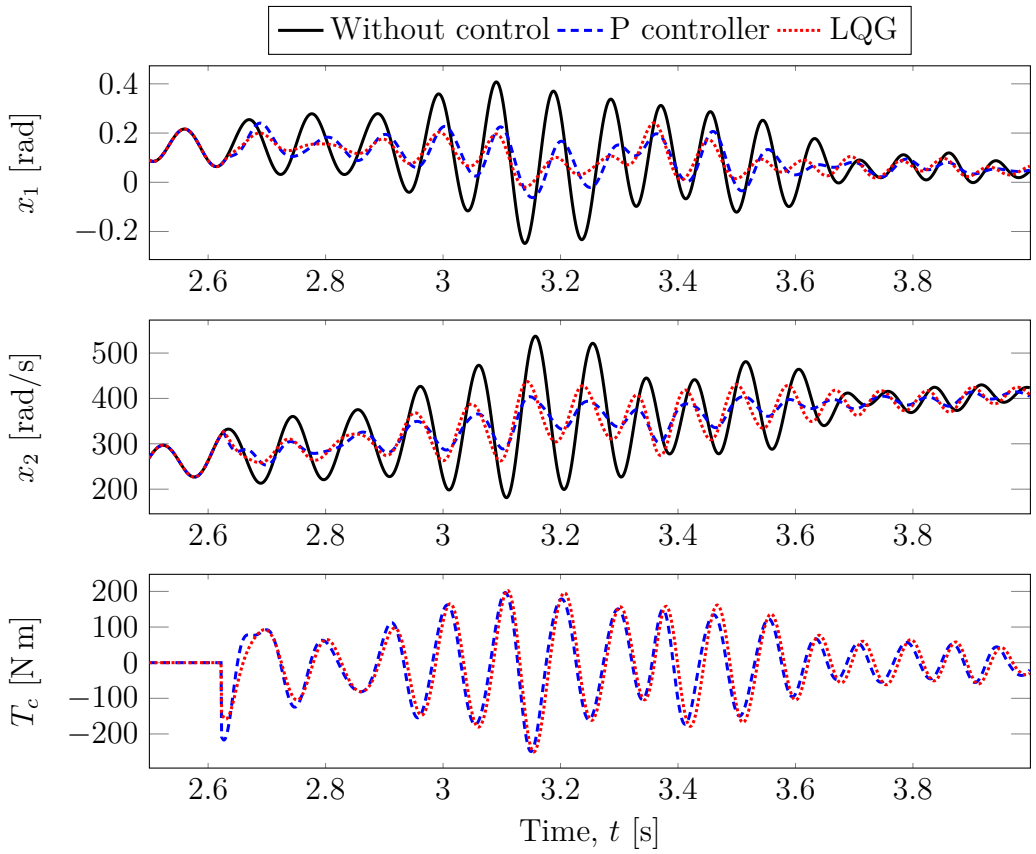

Fig. 4.7. Enlarged section of the high amplitude oscillations presented in Fig. 4.6 for $t = 2.5\,\text{:}4\,\text{s}$. x_1 is the shaft torsion, x_2 is the angular velocity of the EM and T_c is the torque request from the controller.

As can be seen in Fig. 4.7 both controllers are activated just after 2.6 seconds where the oscillations are starting to amplify. The change in the states upon activation seem to be more abrupt in the EM speed (x_2) than in the shaft torsion (x_1), where a more smooth transition is seen. Both controllers reduce the amplitudes of the

oscillations that are intensified in the uncontrolled states. The P controller is better at attenuating the oscillations in the angular velocity of the EM whereas the LQG controller is slightly better at attenuating the oscillations in the shaft torsion.

If looking at the controller outputs (T_c) from Fig. 4.7, it can be seen that the P controller has a more aggressive behaviour upon activation, but then settles in and closely follows the output from the LQG controller. From about 3 seconds and onwards the LQG controller has a slightly higher actuation request and some phase lag, compared to the P controller. The overall behaviour is very similar and none of the signals are close to being saturated in terms of the $\pm 350\,\mathrm{N\,m}$ limit of the EM actuation.

Because both states have a fluctuating average offset it is challenging to precisely determine the amplitude of the oscillations and some approximations are made in order to compare the performance of the controllers. By first turning to the shaft torsion (x_1) for the uncontrolled signal in Fig. 4.7, it is observed that the highest amplitudes of the oscillations occur in the time frame between 3 and 3.2 seconds. Here the average offset of the signal is approximately 0.1 rad. This means that the amplitude of the oscillations in the uncontrolled signal is approximately 0.3 rad. For the LQG and P controllers the equivalent values are 0.09 rad and 0.12 rad respectively. This means that the peak amplitude in the shaft torsion is reduced by 70% for the LQG and 60% for the P controller.

When turning to the EM speed, the highest amplitudes are observed in the same time window, and the approximated peak amplitude for the uncontrolled signal (after subtracting the estimated average) is 200 rad/s. For the LQG controller the same number is 100 rad/s and for the P controller it is 60 rad/s. These figures yield a peak amplitude reduction of the oscillations in the EM speed of 50% for the LQG controller and 70% for the P controller. The peak amplitude reduction for both controllers, in both states, are presented in Table 4.2.

Table 4.2: Approximated controller performance for the reconstructed measurement signal scenario seen in Fig. 4.6 and Fig. 4.7.

Description	**P controller**	**LQG controller**
Peak reduction of x_1	60%	70%
Peak reduction of x_2	70%	50%

As mentioned, it is challenging to calculate the exact amplitude of the oscillations in a scientific way for a signal with a fluctuating average. However, by studying the controllers' behaviour for the signal in Fig. 4.6 it has been shown that the controllers can handle a complex signal without causing undesirable changes in the performance or driveability, also for a signal with oscillations occurring at an offset EM speed. Because this has been demonstrated and no unexpected issues or torque saturations are observed, and in order to allow for more exact calculations, the rest of the analysis is performed on signals without a varying average term and without analysing the torque requests from the controllers.

4.4.2 Damping in the nominal plant

The controllers' response times and abilities to attenuate oscillations of frequencies that coincide with the eigenfrequency of the nominal plant (10 Hz) are analyzed by studying their responses when a sinusoidal wave with amplitude 50 000 N m and frequency 10 Hz is added as a disturbance at the wheel side of the drivetrain. T_{ref} is kept at zero, and the results from the simulation can be seen in Fig. 4.8.

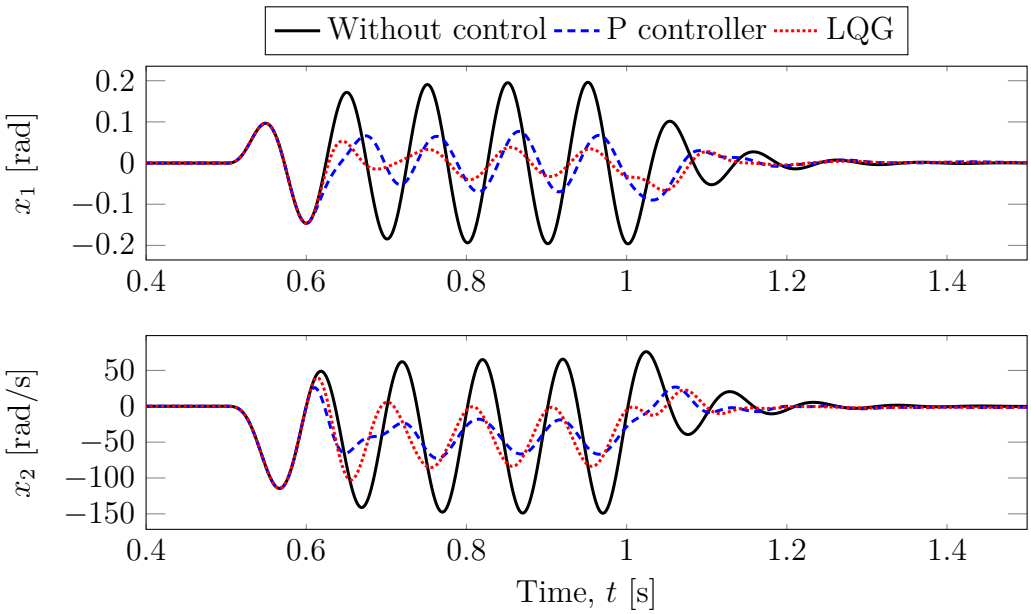

Fig. 4.8. System response when a sinusoidal disturbance with frequency 10 Hz and amplitude 50 000 N m is applied at the wheel. x_1 is the shaft torsion and x_2 is the angular velocity of the EM.

As can be seen in Fig. 4.8, the torsion of the drive shaft (x_1) and the angular velocity of the EM (x_2) in the uncontrolled case starts to resonate while the controlled systems manage to limit the oscillations. The P controller is better at attenuating oscillations in the angular velocity of the EM while the LQG controller is better at reducing the oscillations in the drive shaft torsion. There is no clear difference in the controllers' response times. The achieved active damping, expressed in terms of reduced peak amplitudes in both states, are calculated in the same way as in chapter 4.4.1 and shown in Table 4.3.

Table 4.3: Controller performance for the 10 Hz disturbance scenario seen in Fig. 4.8.

Description	P controller	LQG controller
Peak reduction of x_1	65.8%	82.1%
Peak reduction of x_2	79.8%	62.4%

4.4.3 Varying natural frequency

As previously mentioned, the natural frequency of the real system can vary. In order to verify that the controllers are able to attenuate oscillations even if the eigenfrequency changes with time, the plant model is tuned to have a natural frequency of 8 Hz. This is done by changing the spring constant of the drivetrain model, k_s, from 15 000 Nm/rad to 10 000 Nm/rad, see (2.12). The system with the modified plant is investigated by applying an external load torque with amplitude 50 000 N m and frequency 8 Hz. The results from the simulation can be seen in Fig. 4.9.

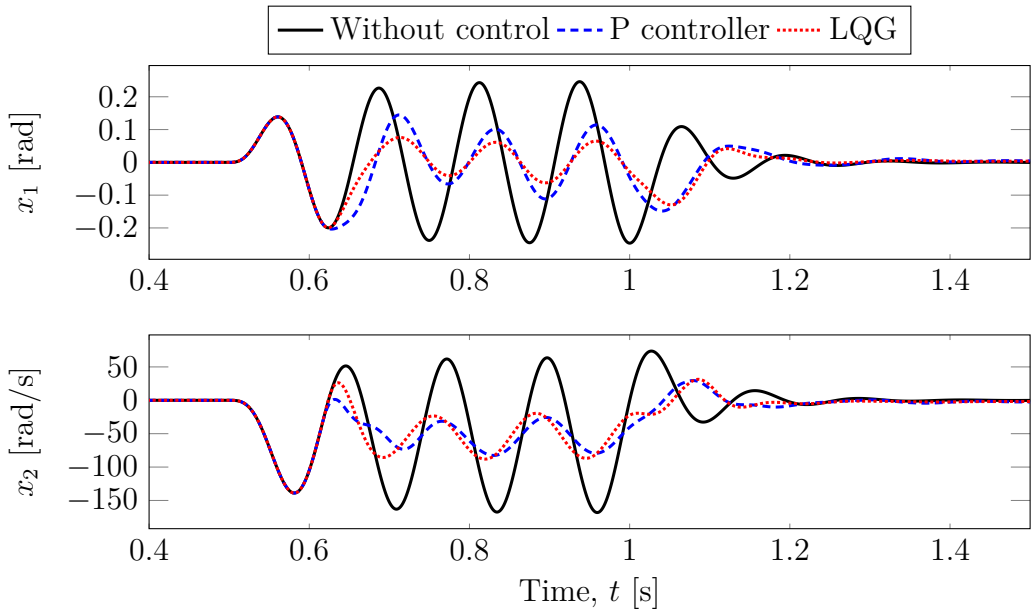

Fig. 4.9. System response when a sinusoidal disturbance with frequency 8 Hz and amplitude 50 000 N m is applied at the wheel. The plant model of the drivetrain has been changed to have an eigenfrequency of 8 Hz. x_1 is the shaft torsion and x_2 is the angular velocity of the EM.

Both the P controller and the LQG controller manage to attenuate the oscillations and avoid resonance also when the natural frequency of the system is changed to 8 Hz. The two controllers have similar responses in the angular velocity of the EM (x_2) while the LQG controller is able to attenuate the torsional oscillations (x_1) more than the P controller. The controllers abilities to reduce the peak magnitude of the oscillations are presented in Table 4.4.

Table 4.4: Controller performance for the scenario seen in Fig. 4.9 where a disturbance of 8 Hz is applied to a plant model with the same natural frequency.

Description	P controller	LQG controller
Peak reduction of x_1	58.3%	74.9%
Peak reduction of x_2	77.1%	71.7%

In the same way as for the 8 Hz case, the natural frequency of the drivetrain is changed to 12 Hz by setting the spring constant k_s equal to 22 500 Nm/rad. The frequency of the applied disturbance is also changed to 12 Hz. The resulting behaviours of the plant and controllers are shown in Fig. 4.10.

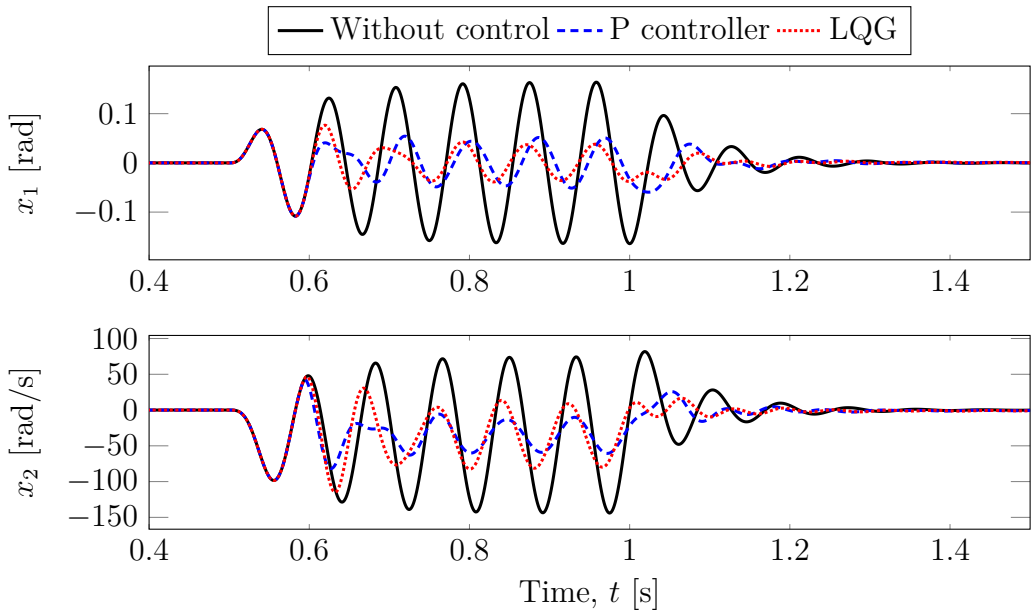

Fig. 4.10. System response when a sinusoidal disturbance with frequency 12 Hz and amplitude 50 000 N m is applied at the wheel. The plant model of the drivetrain has been changed to have an eigenfrequency of 12 Hz. x_1 is the shaft torsion and x_2 is the angular velocity of the EM.

As seen in Fig. 4.10 the controllers manage to reduce the oscillations without becoming unstable in the scenario with a 12 Hz disturbance as well. Also for this case the LQG controller performs better in damping the shaft torsion (x_1) than the P controller, that again reduces the EM speed oscillations (x_2) further than the LQG controller. An increased damping in the shaft torsion, compared to the 8 Hz case, is observed for both controllers. It can also be seen that the LQG controller does not perform as well in reducing the oscillations of 12 Hz as it did for the 8 Hz disturbance. The peak oscillation reductions are presented in Table 4.5.

Table 4.5: Controller performance for the scenario seen in Fig. 4.10 where a disturbance of 12 Hz is applied to a plant model with the same natural frequency.

Description	P controller	LQG controller
Peak reduction of x_1	68.4%	77.4%
Peak reduction of x_2	77.4%	60%

4.4.4 Varying damping coefficient

In a similar way that the shaft stiffness can vary with time and external conditions, so can the damping coefficient c_s. To make sure that the controllers can handle

some variation in the damping of the drivetrain, the plant model is updated with an increased damping coefficient set to 200 Nms/rad. The response of the modified plant is investigated by applying a load torque at the wheel side of the drivetrain with an amplitude of 50 000 N m and frequency of 10 Hz. The responses can be seen in Fig. 4.11.

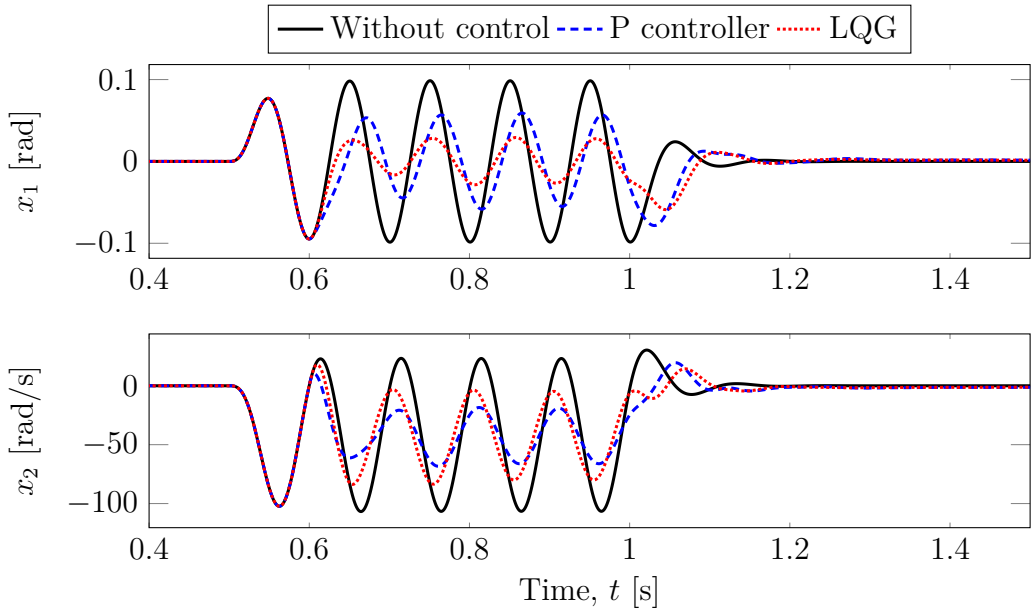

Fig. 4.11. System response when a sinusoidal disturbance with frequency 10 Hz and amplitude 50 000 N m is applied at the wheel. The damping coefficient, c_s, has been changed to 200 Nms/rad in the plant model of the drivetrain. x_1 is the shaft torsion and x_2 is the angular velocity of the EM.

Both controllers are able to attenuate the oscillations in both states. The P controller is better at attenuating oscillations in the angular velocity of the EM (x_2) while the LQG controller is better at reducing the oscillations in the drive shaft torsion (x_1). However, the peak magnitudes are not reduced as much as in the nominal plant, see Fig. 4.8. This is likely a consequence of the oscillations in the uncontrolled signal not reaching as high amplitudes as for the nominal plant, as the plant used in the simulation seen in Fig. 4.11 has a higher damping. This is expected and means that the oscillations in the system are not as severe as in the nominal plant where the damping coefficient is 100 Nms/rad. This also implies that the system does not require as much active damping. The peak reductions for the 200 Nms/rad damping simulation are presented in Table 4.6.

Table 4.6: Controller performance for the scenario seen in Fig.4.11 where a disturbance of 10 Hz is applied to a plant model with the damping coefficient, c_s, set to 200 Nms/rad.

Description	**P controller**	**LQG controller**
Peak reduction of x_1	42.3%	71.8%
Peak reduction of x_2	65.1%	43%

In order to verify that the controllers can also handle a drivetrain with a lower damping coefficient than the nominal plant, the plant model is updated with the damping coefficient, c_s, decreased to 50 Nms/rad. The responses can be seen in Fig. 4.12.

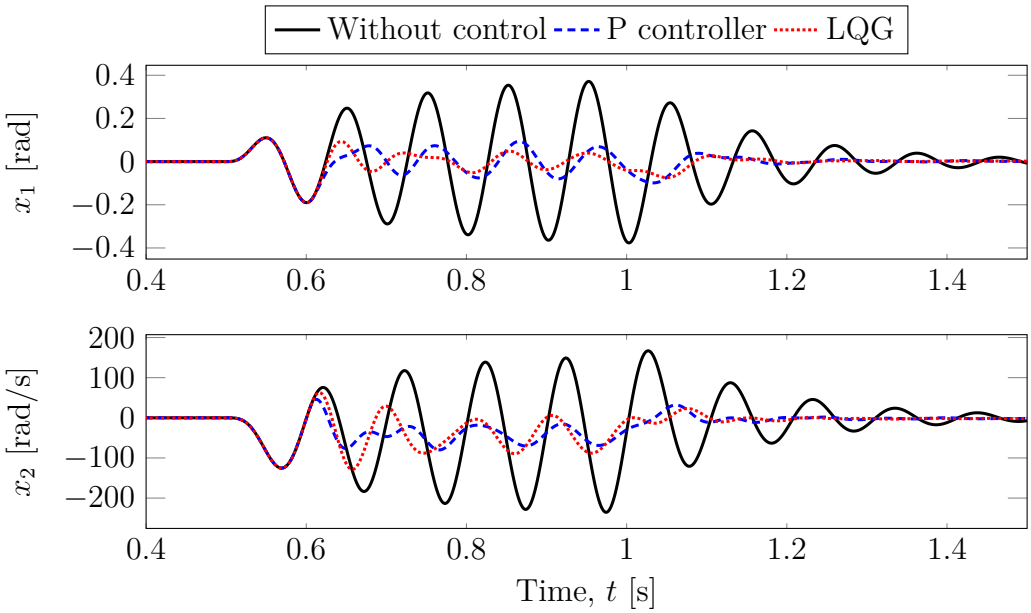

Fig. 4.12. System response when a sinusoidal disturbance with frequency 10 Hz and amplitude 50 000 N m is applied at the wheel. The damping coefficient, c_s, has been changed to 50 Nms/rad in the plant model of the drivetrain. x_1 is the shaft torsion and x_2 is the angular velocity of the EM.

As can be seen in Fig. 4.12 both controllers are able to attenuate the oscillations to a high degree in both states. The oscillations are damped to lower amplitudes than they are for the nominal plant simulation seen in Fig. 4.8, even though the system used in Fig. 4.12 has a lower internal damping than the nominal plant. Or rather, because it has a lower damping, and this causes the load torque to influence the system more and give rise to oscillations with higher amplitudes. The controllers then give higher output signals and are able to achieve greater levels of attenuation. The peak reductions for the 50 Nms/rad damping simulation are presented in Table 4.7

Table 4.7: Controller performance for the scenario seen in Fig. 4.12 where a disturbance of 10 Hz is applied to a plant model with the damping coefficient, c_s, set to 50 Nms/rad.

Description	P controller	LQG controller
Peak reduction of x_1	81.4%	89.3%
Peak reduction of x_2	86.1%	75.1%

A possible issue could be that the controller is disengaged due to the oscillations observed having low amplitudes, and if the disturbance torque acting on the driv-

etrain is still high it could potentially still cause issues if the controller is turned off. However, this has been overcome by setting a relatively low value for when to disengage the controller[†], and by making sure that the oscillations stay below this value for a time corresponding to at least one amplitude peak for oscillations with frequencies down to 5 Hz, see chapter 4.2 (Activation logic). It can also be argued that even if the controller would be disengaged, this means that it has performed its task well and damped the oscillations to values lower than what is considered as critical amplitudes. Furthermore, if the load torque was still at critical levels, the controller would be activated again and keep on performing its intended task.

4.4.5 Varying load inertia

The equivalent inertia of the load (J_l) changes with the weight of passengers, cargo, potential trailer etc. and in order to verify that the controllers can handle these variations, simulations are made where the equivalent mass of the load is changed in the plant model. In Fig. 4.13 the load inertia has been increased from $J_l = 160\,\mathrm{kg\,m^2}$ (in the nominal plant) to $J_l = 320\,\mathrm{kg\,m^2}$. This corresponds to a load mass of $m_l \approx 4750\,\mathrm{kg}$, compared to the 2340 kg used in the nominal plant (see chapter 2.3 and (2.6) for an explanation of how this is calculated). The input to the system is a sinusoidal disturbance of amplitude 50 000 N m and frequency 10 Hz applied at the wheel.

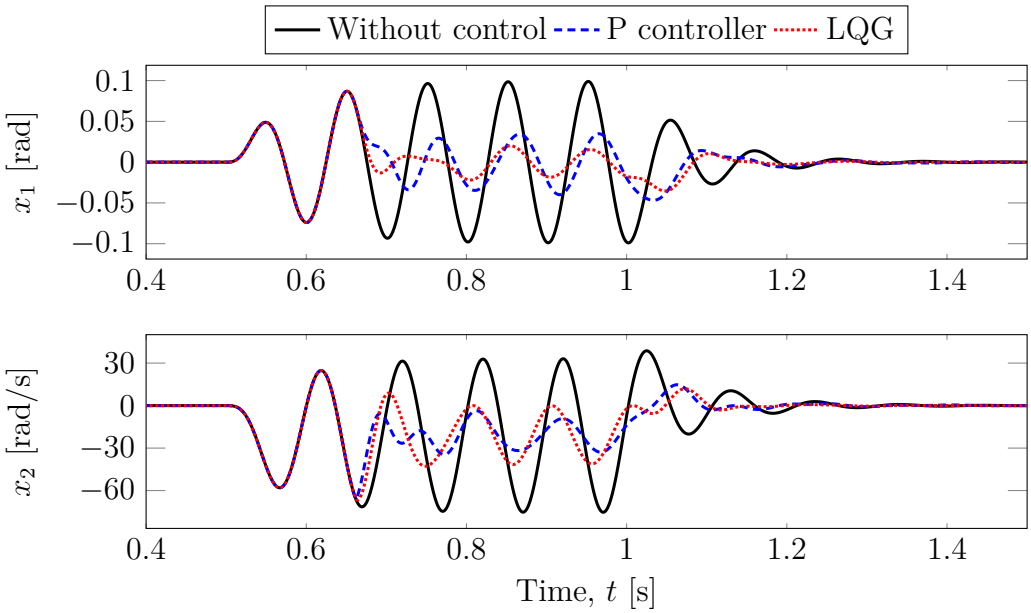

Fig. 4.13. System response when a sinusoidal disturbance with frequency 10 Hz and amplitude 50 000 N m is applied at the wheel. The load inertia, J_l, has been changed to $320\,\mathrm{kg\,m^2}$ in the plant model of the drivetrain. x_1 is the shaft torsion and x_2 is the angular velocity of the EM.

[†]Note that this is not done only for this case, but the activation logic has been tuned to always have this behaviour, so that the controller is not disengaged until the oscillations are damped to levels considered to be sufficiently low. All of the simulations presented in chapter 4.4 use the same activation logic.

As can be seen from Fig. 4.13 the controllers still perform well when the inertia has been doubled, however they are activated slightly later than they are for the nominal load inertia, see Fig. 4.8. This is because the disturbance has a smaller impact on both the shaft torsion (x_1) and the EM speed (x_2) as the load torque is subject to a much larger inertia. Due to the amplitudes of the oscillations not being as high as in the nominal plant, the need for control action is decreased. The level of peak amplitude attenuation that the controllers achieve are very similar to the ones for the nominal plant (presented in Table 4.3) and can be seen in Table 4.8.

Table 4.8: Controller performance for the scenario seen in Fig. 4.13 where a disturbance of 10 Hz is applied to a plant model with the load inertia, J_l, set to 320 kg m^2.

Description	P controller	LQG controller
Peak reduction of x_1	64.9%	84.4%
Peak reduction of x_2	78%	61.4%

4.4.6 Frequency sweep

In order to gain a better understanding of how the controlled system behaves, the nominal plant model is exposed to an external load torque with amplitude 50 000 N m and a frequency increasing from 0 to 20 Hz. The responses can be seen in Fig. 4.14.

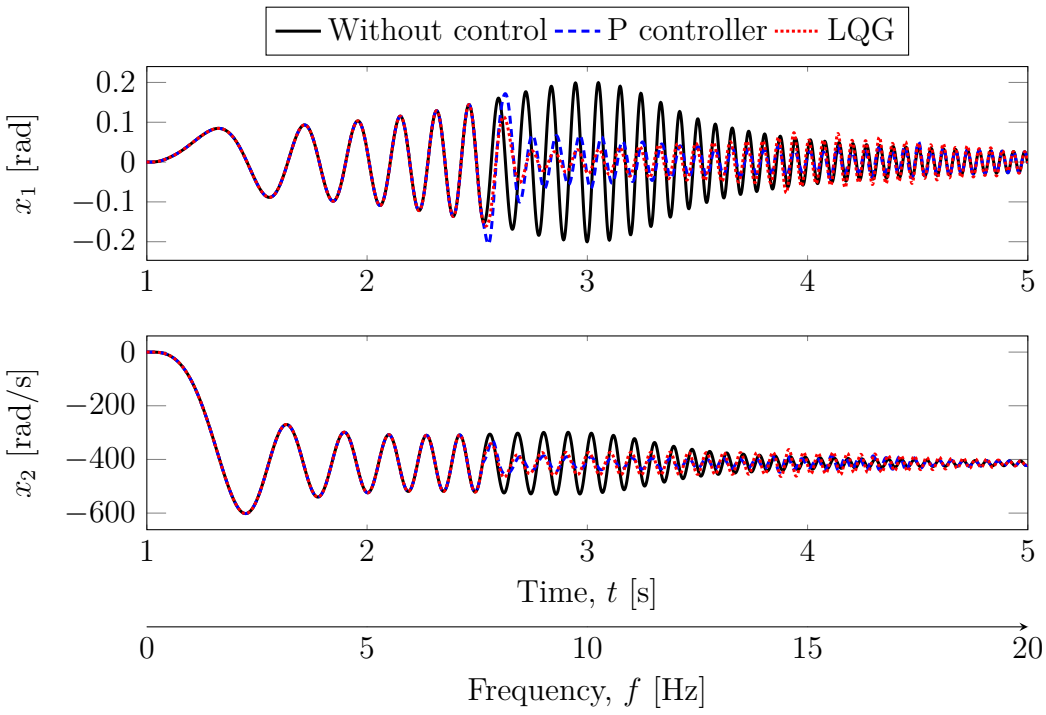

Fig. 4.14. Controller performance for a disturbance with a frequency sweeping from 0 to 20 Hz applied to the nominal plant model. x_1 is the shaft torsion and x_2 is the angular velocity of the EM.

From Fig. 4.14 it is observed that the torsion in the drive shaft (x_1) does indeed seem to resonate for frequencies in the region of $8-12\,\text{Hz}$, where the amplitudes are magnified the most. Note that the amplitude of the disturbance is constant at $50\,000\,\text{N m}$, but that the amplitude of the oscillations in both states have varying amplitudes depending on the frequency. By looking at the EM speed (x_2) it is observed that the lower frequencies have as high, if not higher, magnitude gains as the frequencies that affect the torsion of the drive shaft the most. As stated in the analysis of the drivetrain (see chapter 2.4) this makes it challenging to observe resonance in the shaft torsion by only measuring the EM speed, due to the lack of amplification in the critical frequencies. By incorporating the RLS algorithm in both controllers, but also in the activation logic, this issue is overcome. This can be seen by studying the controlled shaft torsion where both controllers seem to engage and damp the oscillations considerably in the region of the critical frequencies.

The LQG controller seems to be generating some small overshoots in both states for frequencies above $\sim 14\,\text{Hz}$. Because they are small in the context they are not considered to be potentially harmful to the drive shaft, however, in order to verify that they are not causing any issues related to driveability the output wheel speed from the LQG-controlled plant is studied for $t = 3.5:5\,\text{s}$, and this can be seen in Fig. 4.15.

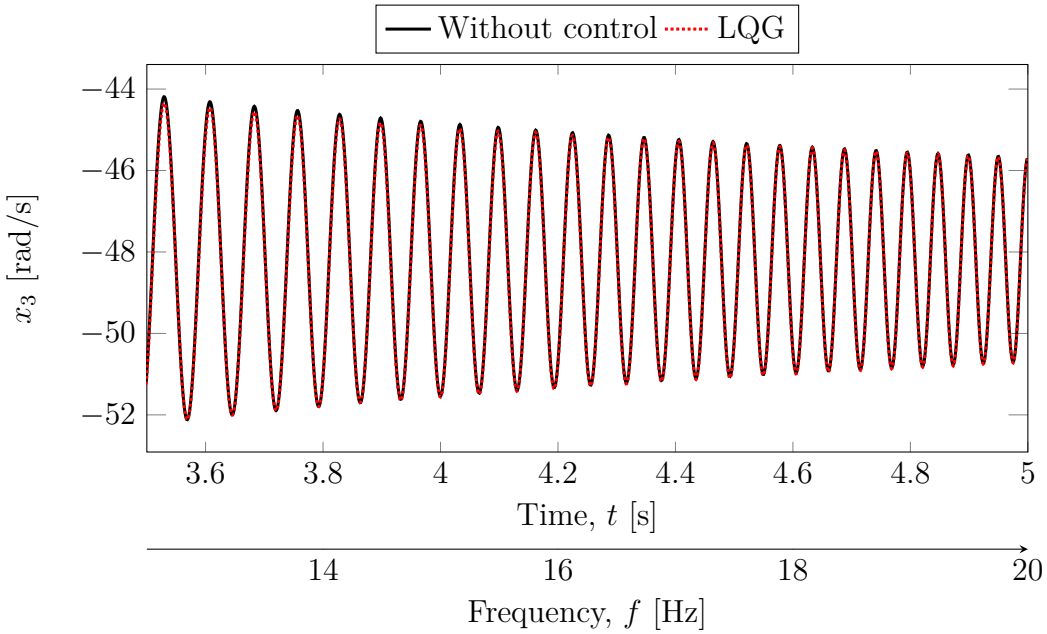

Fig. 4.15. Wheel speed corresponding to the case studied in Fig. 4.14. The frequency is increased with time.

As can be seen in Fig. 4.15 the LQG-controlled wheel speed aligns almost perfectly with the uncontrolled wheel speed. Thus the marginal overshoots generated by the LQG controller seen in Fig. 4.14 are considered harmless and to not cause any issues in regards to driveability.

The controllers' individual behaviours concerning the EM speed and the torsion in the drive shaft are studied more closely by zooming in on the region of Fig. 4.14 containing the critical frequencies. The zoomed in snapshot for $f = 7.5:12.5\,\text{Hz}$ can be seen in Fig. 4.16.

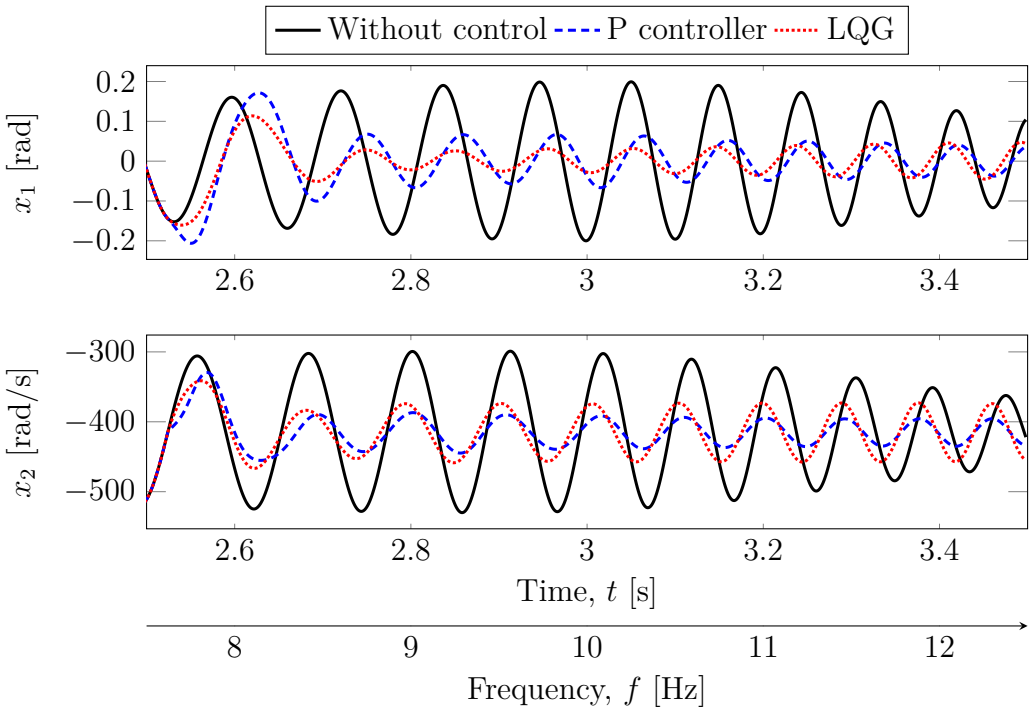

Fig. 4.16. Snapshot of the oscillations presented in Fig. 4.14 for $f = 7.5:12.5\,\text{Hz}$. x_1 is the shaft torsion and x_2 is the angular velocity of the EM.

When looking at the controlled states in Fig. 4.16 the trend seen in the rest of the analysed cases is repeated. The LQG achieves higher levels of attenuation in the shaft torsion whereas the P controller is able to further dampen the EM speed oscillations. The reduction in the peak amplitude oscillations are presented in Table 4.9.

Table 4.9: Controller performance for the scenario seen in Fig. 4.14 and Fig. 4.16 where a disturbance with a frequency sweeping from $0-20\,\text{Hz}$ is applied to the nominal plant model.

Description	**P controller**	**LQG controller**
Peak reduction of x_1	68.3%	84.0%
Peak reduction of x_2	78.4%	63.3%

In Fig. 4.16 it can be seen that the controllers are activated at $f \approx 7.7\,\text{Hz}$. This is a consequence of the RLS not being an ideal filter, leading to some leakage from the frequencies in the regions of the passband. As stated in [21], it is impossible to design an ideal filter, i.e. with a gain of at least unity in the passband and a constant gain of zero in the stopband. There are no identified issues related to the controllers being activated at $f \approx 7.7\,\text{Hz}$, it is rather considered to add some margin.

4.5 Summary

Two control strategies with integrated RLS algorithm and auxiliary activation logic have been implemented in Simulink together with a model of the EM and plant. The two controllers have different levels of complexity, where the P controller is independent of the plant model and only uses a proportional gain constant to achieve reduction of the EM speed oscillations. The LQG controller uses a model of the drivetrain plant in order to attenuate oscillations in all three states of the state space model.

The activation logic that is proposed uses two different thresholds for when to engage and disengage the controllers and thereby limits the range of scenarios for when the controllers are active. This is implemented in order to ensure that the controllers are engaged only when necessary to guarantee performance and driveability. This also means that the target of the controllers, which is to completely attenuate the oscillations, is limited to the following: lower the oscillations to the level of the deactivation threshold, D_{th}.

The analysis shows that both the P controller and LQR controller can achieve active damping of oscillations in the drivetrain for the specified frequency range of $8-12\,\text{Hz}$ without compromising the performance or driveability. Furthermore, they also do so for the studied changes in the drivetrain parameters and are considered to be robust to variations in the plant model and external conditions. The LQR controller consistently shows better performance when it comes to damping the peak amplitude oscillations in the torsion of the drive shaft, whereas the P controller is able to reduce the peak amplitudes of the EM speed oscillations to a higher degree in all of the studied scenarios. The average achieved peak amplitude reduction, for all of the presented scenarios, is calculated and can be seen in Table 4.10.

Table 4.10: Average peak reduction for the results presented in Table 4.2-4.9.

Description	P controller	LQG controller
Peak reduction of x_1	63.7%	79.2%
Peak reduction of x_2	76.5%	60.9%

According to the average peak reduction the LQG controller damps the oscillations in the drive shaft torsion 15.5 percentage points more than the P controller, which damps the EM speed oscillations 15.6 percentage points more than the LQG controller.

5
Discussion

The performance of the signal estimation method has a big impact on the results that can be achieved through the active damping controller. It is possible that there exists a strategy better suited than the RLS algorithm, which was ultimately chosen, and that by putting more effort into finding the ultimate method even higher oscillation reduction could be achieved. However, some limitations had to be made concerning the scope of methods to be investigated due to time restraints. The RLS algorithm proved to be successful in capturing the characteristics of interest and furthermore to be easy to tune and manipulate to achieve a desirable behavior. An area for possible improvement is the low frequency rejection that showed to not be optimal in the RLS filter, when compared to the DFT method, for the oscillating ramp (see chapter 3.5.2).

The results from the analysis of the controllers indicate that it is possible to reduce the oscillations in a drivetrain by only measuring the angular velocity of the EM. The P controller seems to be the best, out of the two investigated controllers, at attenuating the EM speed oscillations, while the LQG controller has better performance in reducing the torsion in the drive shaft. Although the LQG controller manages to attenuate the torsion in the drive shaft, which is considered to be the ultimate goal, to a higher degree than the P controller, the P controller has other advantages. Because it does not require a model, it is easier to implement in a real vehicle. It also means that the P controller could be used in several different vehicles without having to take their dynamics into account. The P controller would also require less real time computations which is an additional possible benefit, however it could be argued that this is not a concern due to the high capacity of today's microprocessors.

The phase of the control signal seems to have a big impact on the attenuation of the oscillations in the drive shaft torsion. If the torque delivered by the EM would mirror the corresponding torque in the drive shaft perfectly it should be possible to attenuate the oscillations to a higher degree than what has been observed. Unfortunately, it is difficult to predict what phase the control signal should have as it varies with the model parameters and the frequency of the disturbance. The LQG controller uses all model states to generate the control signal and thereby it manages to create an output with a phase that yields a better result than the P controller. However, the Kalman filter seems to have shortcomings in estimating the phase in the angular velocity of the wheel, and thus this is a possible area for improvement.

A possible weakness that could be pointed out in the robustness analysis is that it does not cover combinations of variations in the parameter values defining the plant model. As it would practically be impossible to present the performance of the control strategies in all possible combinations of variations, only certain cases considered to be representative were presented to show how the control strategies behave in extreme cases for single parameter variation. This was done because it would be hard to justify why certain combinations of variations were presented and not others. However, hundreds of different combinations that are considered to be rather extreme, i.e. corner cases, have been studied and no potential issues were found. In order to allow for analysing the cause-effect relationship, only cases where one parameter was changed at a time have been presented.

5.1 Sustainability and ethical aspects

Goal 13 of the United Nations sustainable development goals states that "2019 was the second warmest year on record and the end of the warmest decade (2010-2019) ever recorded. Carbon dioxide (CO_2) levels and other greenhouse gases in the atmosphere rose to new records in 2019. Climate change is affecting every country on every continent. It is disrupting national economies and affecting lives. Weather patterns are changing, sea levels are rising, and weather events are becoming more extreme" [22]. It furthermore says that we must invest in sustainable solutions, that fossil fuel subsidies must end and that polluters must pay for their pollution. To address the climate emergency we need to trigger long-term systematic shifts that will change the trajectory of CO_2 levels in the atmosphere.

About 14% of all CO_2 emissions in the European Union come from cars [23]. The CO_2 emissions of an ICE car is approximately 4.5 times higher than for an electric car charged with renewable produced electricity [24]. As this project aims at reducing mechanical stress in the drivetrain of xEVs, it may yield a positive contribution in the required transition as the world moves away from vehicles running on fossil fuels. By reducing component wear and the risk for drive shaft breakage it could increase the lifetime of the vehicle and drivetrain components and thereby help reducing material usage. Substituting a physical oscillation damper with software such as an active controller, could further decrease material usage and component costs. By eliminating the physical damper, weight and energy consumption is reduced, leading to improved range, which is the factor most cited in deciding what xEV to buy [25].

6
Conclusion

The possibility to damp potentially harmful mechanical oscillations in an xEV drivetrain, caused by external load torque transients, by measuring only the EM speed and actively controlling the torque input from the EM has been investigated.

6.1 Results from present work

Known vehicle dynamics were used to represent a drivetrain as a two mass spring damper system and put into a linear third order state-space model, which showed to capture the resonance in the drive shaft for load torques coinciding with the natural frequency of the drivetrain ($8-12\,\mathrm{Hz}$).

Four different methods for distinguishing the oscillatory component within a certain frequency range of a signal were investigated and compared in order to find a technique suited for an active drivetrain oscillation damping controller. The RLS algorithm showed the most promising results in terms of quickly gaining amplitude and following a signal with varying frequency and was ultimately considered to be the best overall signal estimation method for the intended application.

Two controllers were developed and implemented together with the RLS algorithm. One of the controllers, the P controller, is a simple proportional gain controller that does not require any information about the dynamics of the drivetrain and outputs a control torque to reduce oscillations in the EM speed. The other controller, the LGQ controller, uses a model of the drivetrain in order to estimate and compensate for the oscillations in the drive shaft torsion, EM speed and in the wheel speed. Both controllers were implemented in the full system with the model of the EM and drivetrain plant. The controllers generate an active damping torque to compensate for oscillations with amplitudes exceeding $10\,\mathrm{rad/s}$ within $8-12\,\mathrm{Hz}$. By using an auxiliary activation logic for engaging and disengaging the controller the tractive torque to drive the vehicle is not unnecessarily affected, nor is the driveability experienced by the passenger.

For the investigated scenarios the P controller achieved an average peak amplitude reduction of 63.7% in the drive shaft torsion and 76.5% in the EM speed oscillations, compared to the uncontrolled case. The LQG controller was able to reduce the peak amplitudes by 79.2% in the oscillations of the drive shaft torsion and 60.9% for the EM speed.

6.2 Recommended future work

During the project all simulations have been performed using a linear third order model to investigate the controllers performance. To get a deeper understanding of how the controllers behave it would be of interest to implement them with a more complex model of higher order but also to verify the results through tests performed in a real vehicle.

As it has been shown that low frequencies from the load torque have high magnitude gain to the observed EM speed measurement (see Fig. 2.3), the behaviours of the controllers and activation logic should be studied thoroughly for low frequency load torques applied in a physical system to ensure that the controllers are not activated in the case of e.g. emergency braking, as this could be recognised as a high amplitude, low frequency load torque.

The phase of the control signal seems to be significant for oscillation attenuation, and it would therefore be interesting to investigate this relationship further. There is a phase shift between the measured angular velocity of the EM and an optimal control torque input. This phase varies with the frequency of the oscillations. A possible improvement to the developed controllers could therefore be to implement a phase-gain map that connects the frequencies of the oscillations to the optimal phase of the control torque signal.

Bibliography

[1] Volvo Cars Company, "The future is electric." https://group.volvocars.com:443/company/innovation/electrification, (Accessed 2021-01-22).

[2] G. Götting and M. Kretschmer, "Development and series application of a vehicle drivetrain observer used in hybrid and electric vehicles," in *2013 World Electric Vehicle Symposium and Exhibition (EVS27)*, 2013, pp. 1–9.

[3] A. Scamarcio, P. Gruber, S. De Pinto, and A. Sorniotti, "Anti-jerk controllers for automotive applications: A review," *Annual Reviews in Control*, vol. 50, 07 2020.

[4] M. Pettersson, "Driveline modelling and control," Ph.D. dissertation, Linköping University, 1997.

[5] J. Sainio, "Backlash compensation in electric vehicle powertrain," Master's thesis, Aalto University, 2016.

[6] C. Mo, A. Beaumount, and N. Powell, "Active control of driveability," *SAE Technical Papers*, 02 1996.

[7] O. Atabay, M. Ötkür, and İsmail M Ereke, "Model based predictive engine torque control for improved drivability," *Proceedings of the Institution of Mechanical Engineers, Part D: Journal of Automobile Engineering*, vol. 232, no. 12, pp. 1654–1666, 2018.

[8] H. Zumbahlen *et al.*, *Linear circuit design handbook*. Newnes, 2011.

[9] P. V. Brennan, *Phase-locked loops: Principles and Practice*. Palgrave, London, 1996.

[10] Z. Zhang, Y. Yang, R. Ma, and F. Blaabjerg, "Zero-voltage ride-through capability of single-phase grid-connected photovoltaic systems," *Applied Sciences*, vol. 7, p. 315, 03 2017.

[11] M. Ciobotaru, R. Teodorescu, and F. Blaabjerg, "A new single-phase pll structure based on second order generalized integrator," in *2006 37th IEEE Power Electronics Specialists Conference*, 2006, pp. 1–6.

[12] S. Golestan, M. Monfared, F. D. Freijedo, and J. M. Guerrero, "Dynamics assessment of advanced single-phase pll structures," *IEEE Transactions on Industrial Electronics*, vol. 60, no. 6, pp. 2167–2177, 2013.

[13] E. W. Hansen, *Fourier transforms: Principles and Applications*. Hoboken, New Jersey: John Wiley and Sons, Incorporated, 2014.

[14] M. Beza and M. Bongiorno, "A fast estimation algorithm for low-frequency oscillations in power systems," in *Proceedings of the 2011 14th European Conference on Power Electronics and Applications, EPE 2011*, 10 2011, pp. 1 – 10.

[15] M. Beza and M. Bongiorno, "Application of recursive least square (rls) algorithm with variable forgetting factor for frequency components estimation in a generic input signal," in *2012 IEEE Energy Conversion Congress and Exposition (ECCE)*, 2012, pp. 2164–2171.

[16] M. Beza, "Control of energy storage equipped shunt-connected converter for electric power system stability enhancement," Ph.D. dissertation, Chalmers University of Technology, 06 2012.

[17] J. Fredriksson, H. Weiefors, and B. Egardt, "Powertrain control for active damping of driveline oscillations," *Vehicle System Dynamics*, vol. 37, no. 5, pp. 359–376, 2002.

[18] H. Latorre and L. Angquist, "Analysis of tcsc providing damping in the interconnection colombia-ecuador 230 kv," in *2003 IEEE Power Engineering Society General Meeting (IEEE Cat. No.03CH37491)*, vol. 4, 2003, pp. 2361–2361.

[19] M. Berriri, P. Chevrel, D. Lefebvre, and M. Yagoubi, "Active damping of automotive powertrain oscillations by a partial torque compensator," in *2007 American Control Conference*, 2007, pp. 5718–5723.

[20] L. Ljung, *Control theory: multivariable and nonlinear methods*. Taylor & Francis, 2000.

[21] B. Meddins, "Chapter 4 - the design of iir filters," in *Introduction to Digital Signal Processing*. Oxford: Newnes, 2000, pp. 71–101.

[22] United Nations, "Sustainable development goals: Goal 13: Take urgent action to combat climate change and its impacts." https://www.un.org/sustainabledevelopment/climate-change/, (Accessed 2021-06-06).

[23] European Parliament, "Co2 emissions from cars: facts and figures," https://www.europarl.europa.eu/news/en/headlines/society/20190313STO31218/co2-emissions-from-cars-facts-and-figures-infographics, (Accessed 2021-06-06).

[24] K. Holmberg and A. Erdemir, "The impact of tribology on energy use and co2 emission globally and in combustion engine and electric cars," *Tribology International*, vol. 135, pp. 389–396, 2019.

[25] Forbes, "Range anxiety is very real, new j.d. power evs survey finds," https://www.forbes.com/wheels/news/range-anxiety-very-real-jd-power-evs-survey/, (Accessed 2021-06-06).

DEPARTMENT OF ELECTRICAL ENGINEERING
CHALMERS UNIVERSITY OF TECHNOLOGY
Gothenburg, Sweden 2021
www.chalmers.se

CHALMERS
UNIVERSITY OF TECHNOLOGY